Biogeosciences, 22, 3821–3842, 2025
https://doi.org/10.5194/bg-22-3821-2025

Biogeosciences Open Access EGU

Lake anoxia, primary production, and algal community shifts in response to rapid climate changes during the Late Glacial

Stan J. Schouten[1,2], **Noé R. M. M. Schmidhauser**[1,2], **Martin Grosjean**[1,2], **Andrea Lami**[3], **Petra Boltshauser-Kaltenrieder**[1,4], **Jacqueline F. N. van Leeuwen**[1,4], **Hendrik Vogel**[1,5], **and Petra Zahajská**[1,2]

[1]Oeschger Center for Climate Change Research, Universität Bern, Hochschulstrasse 4, 3012 Bern, Switzerland
[2]Institute of Geography, Universität Bern, Hallerstrasse 12, 3012 Bern, Switzerland
[3]Water Research Institute (CRN-IRSA), Unit Verbania, Viale Tonolli 50, 28922 Verbania, Italy
[4]Institute of Plant Sciences, Universität Bern, Altenbergrain 21, 2013 Bern, Switzerland
[5]Institute of Geology, Universität Bern, Baltzerstrasse 1, 3012 Bern, Switzerland

Correspondence: Stan J. Schouten (stan.schouten@unibe.ch)

Received: 30 January 2025 – Discussion started: 18 February 2025
Revised: 23 April 2025 – Accepted: 11 May 2025 – Published: 7 August 2025

Abstract. Lakes around the world are facing growing threats from climate change and human impacts. Rising temperatures and increased nutrient levels are causing eutrophication and deoxygenation, harming freshwater resources and the essential ecosystem services they provide. While modern impacts are well studied, knowledge on the responses of lake ecosystems to climate change in pre-anthropogenic times is still sparse. Current studies often rely on models or short observation time series, making it challenging to isolate the effects of warming from other factors. Lake sediments provide long-term records to study these effects in times prior to anthropogenic impact.

We investigate the responses of aquatic primary production, lake stratification, and deoxygenation to rapid climate change during the Late Glacial (18–11 ka cal BP) using hyperspectral imaging, pigment extractions, XRF, and sequential extraction of redox-sensitive P, Mn, and Fe in a small kettle hole lake (Amsoldingersee, Switzerland).

Our record reveals that ice cover was the primary driver of hypolimnetic anoxia, while the availability of nutrients determined the composition of algal communities. Four anoxic phases occurred in cold periods with prolonged ice cover: (i) Heinrich 1 (ca. 16.1 ka cal BP), (ii) the Aegelsee Oscillation, (iii) the Gerzensee Oscillation, and (iv) the Younger Dryas. Aquatic primary production and algal communities already responded to initial relatively weak warming during Heinrich 1 (16.1 ka cal BP) long before the rapid Bølling warming and synchronously to rapid climatic changes during Late Glacial times. Responses of the algal community to temperature were strongly modulated by nutrient limitations (P, N, and Si), which have varying importance over time, with dust and volcanic tephra (Laacher See) being major nutrient sources. Anoxic phases changed the algal communities, but these shifts were found to be reversible once the anoxia disappeared. Further, the sediments of Amsoldingersee provide a continuous record of atmospheric dust deposition (Ti, Zr, Si) covering the entire Late Glacial period. The similarity with the NGRIP dust record supports the view that the same large-scale atmospheric circulation regime controlled central Europe (Switzerland) and Greenland.

1 Introduction

The combined effects of climate warming and anthropogenic eutrophication prompt lake stratification and oxygen depletion, threatening freshwater ecosystems globally (Jansen et al., 2024; Jane et al., 2021; Weyhenmeyer et al., 2024). It is acknowledged that climate change, nutrient loading (N, P), and biodiversity loss have crossed the limits of planetary boundaries (Richardson et al., 2023). The effects of eutrophication on lake ecosystems are broad, including water quality deterioration, fish kills, algal blooms, and cyanobacteria blooms, sometimes releasing cyanotoxins that threaten human health directly (Lévesque et al., 2014).

Oligotrophic lakes are particularly sensitive to both increasing temperatures and increasing nutrient loads (Vinnå et al., 2021), and, throughout the last decades, many of these lakes have already transitioned into eutrophic stratified aquatic ecosystems with hypolimnetic anoxia (Jenny et al., 2016; Klanten et al., 2023; Jansen et al., 2024). Persistent bottom water anoxia and reducing conditions may promote efficient nutrient recycling within the water column, which may sustain eutrophication through chemical feedback once eutrophication is established (Schaller and Wehrli, 1996; Gächter et al., 1988; Carey et al., 2022; Hupfer and Lewandowski, 2008; Nürnberg, 1998). Eutrophication promotes generalist species competitiveness over specialists adapted to ecological niches in oligotrophic settings, leading to algal community shifts. Furthermore, the associated deoxygenation of the water column leads to rapid, unidirectional shifts in biological communities (Bush et al., 2017), suggesting that the consequences of anoxia might even be irreversible (Carey et al., 2022).

It is increasingly recognised that rapid climate warming is an essential driver of freshwater and ecosystem deterioration (Meerhoff et al., 2022; Jane et al., 2021; Jeppesen et al., 2010). Climate warming mostly affects nutrient loading to lakes through changes in the watershed dynamics, e.g., by affecting hydrological patterns, weathering rates, and mass fluxes. However, it is unclear under which conditions climate warming leads to anoxia, particularly in temperate and cold environments. This is due to (i) the complexity of factors controlling lake mixing and seasonal stratification (winter or summer), lake morphometry, vegetation, and climate and (ii) the lack of long-term records on anoxia and its drivers (Friedrich et al., 2014). Most studies assessing the impacts of climate warming on primary production, anoxia, or algal communities are based on in situ experiments, observations during short periods of time, or model simulations (Salk et al., 2022; Foley et al., 2012; Gilarranz et al., 2022). However, because climate warming and nutrient availability covary in the instrumental period, the different driving factors are hard to disentangle within short observational datasets. A long-term perspective is needed, and lake records provide a convenient solution.

Periods of rapid climate warming in the past can provide empirical information on lake physical and biogeochemical responses to rapid climate warming under pre-anthropogenic conditions, when the confounding effects of anthropogenic eutrophication were absent. In the north-western Europe, the Late Glacial period (ca. 18–11 ka cal BP) provides an ideal setting with rapid high-amplitude warmings and coolings within decades during one Dansgaard–Oeschger cycle (Rasmussen et al., 2014) to study lake responses under pre-anthropogenic conditions.

Accordingly, our research is driven by the following questions:

1. How did lake mixing regimes, nutrient availability, primary production (PP), and anoxia respond to rapid climate change during the Late Glacial period?

2. Can we identify the importance of drivers for PP, anoxia, and algal communities through time?

3. Were the algal community shifts reversible once the stressor disappeared and, if so, at what timescales?

To answer these questions, we investigate a sediment core from a small kettle hole lake on the Swiss Plateau, Amsoldingersee, using a multiproxy approach. This lake is located adjacent to Gerzensee in an area that responded in extraordinary detail to Late Glacial climatic changes documented in the North Atlantic domain and Greenland (Eicher, 1987; Lotter et al., 1992; Ammann et al., 2013). Amsoldingersee contains the complete Late Glacial sediment sequence, including early deglacial anoxic periods (Lotter and Boucherle, 1984).

2 Study site

Amsoldingersee (4°43′ N, 07°34′ E; 641 m a.s.l.) is an endorheic, currently eutrophic, small (38 ha; 13 m deep) lake on the shoulder of the Aare Valley, located in the Swiss Plateau (Fig. 1b). The kettle hole lake (Lotter and Boucherle, 1984) was formed in a drumlin landscape after the collapse of the Last Glacial Aare glacier (Fabbri et al., 2018). Basal ages of deglacial lakes in the region range between 19.1 and 17.7 ka cal BP (Rey et al., 2020). A moraine dammed the lake, forming a 2 m high sill (Fig. 1c), which leads into an incised valley. Studying a near-shore core, Lotter and Boucherle (1984) found that Late Glacial sediments were preserved, except for a hiatus in the Younger Dryas. This hiatus in littoral sediments was interpreted as lake levels > 3 m lower than today, suggesting lake level fluctuations in the past. The catchment (4.74 km^2) consists of a southeastern sloping drumlin field with glacial carbonaceous till on top of Jurassic limestone in the south and Oligocene molasse in the north. Until the 19th century, the lake was surrounded by extended wetlands (Lotter and Boucherle, 1984; Guthruf et al., 2015). Substantial postglacial erosional features are not observed, suggesting that the hydrological catchment remained unchanged. The lake catchment is disconnected from a significant river system; the lake receives water from rain, surface runoff, and subsurface runoff. Throughout the Late Glacial (ca. 18–11 ka cal BP), the vegetation in the catchment developed from a steppe tundra to a pine forest (Rey et al., 2020). Today, agriculture and grasslands are the dominant land use (Guthruf et al., 2015). The lake hosts a suite of algae, including Chlorophyceae, Bacillariophyceae, Chrysophyceae, Cryptophyceae, cyanobacteria, and anoxigenic bacteria (Guthruf et al., 2015).

The climate today is warm temperate (Cbf) with 9 °C annual mean temperature and 19 °C in July (MeteoSwiss). In

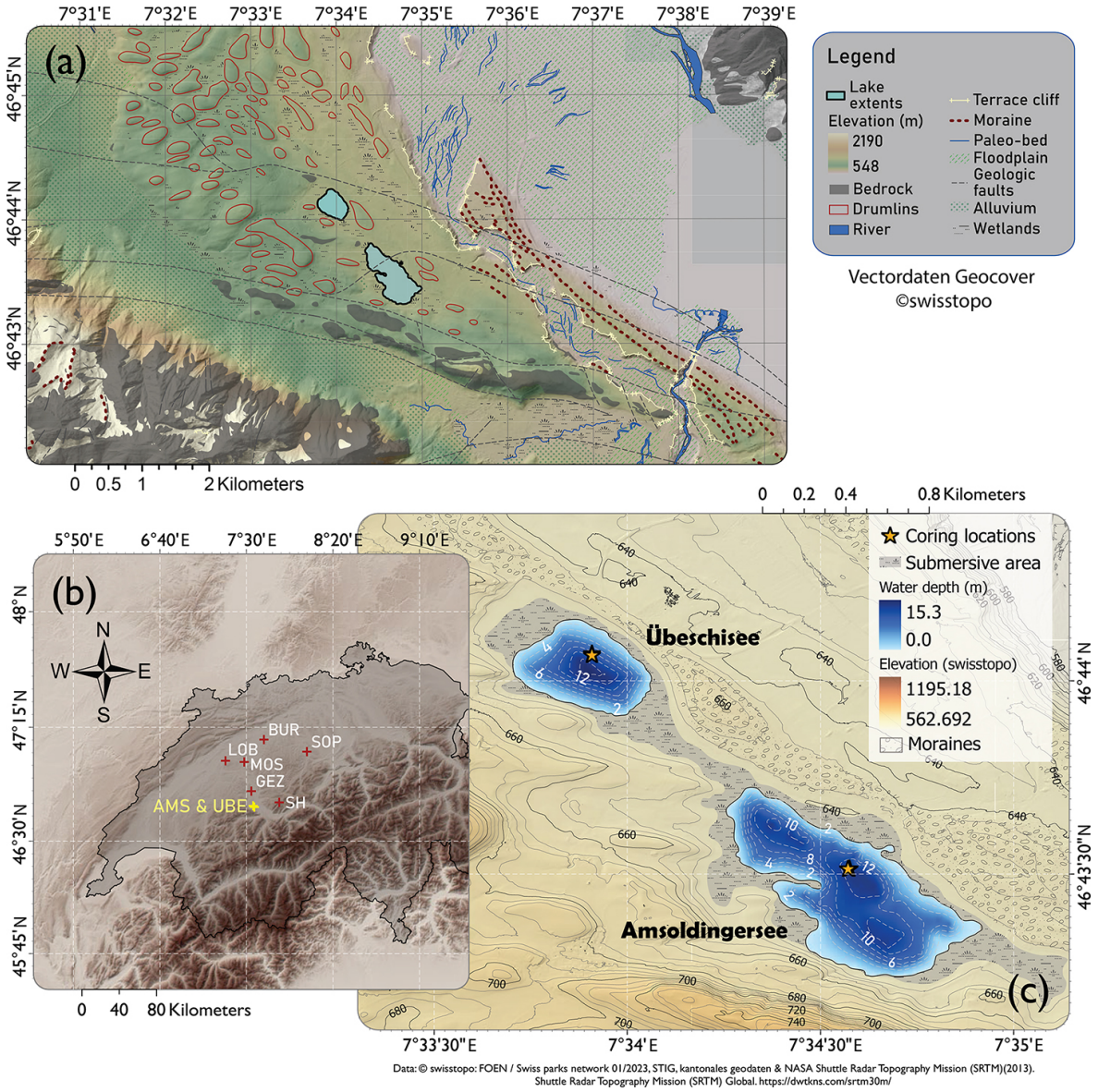

Figure 1. **(a)** Geomorphology around Amsoldingersee (drumlins, floodplains, moraines). **(b)** Topographic map (NASA SRTM) of the northwestern Alps with study sites mentioned in the text: SH, Sieben Hängste speleothem; GEZ, Gerzensee; MOS, Moossee; LOB, Lobsigensee; BUR, Burgäschisee; and SOP, Soppensee. **(c)** Geomorphological map of the catchment area of Amsoldingersee and Übeschisee with bathymetry.

contrast, the Late Glacial climate was initially very cold and dry, with annual temperatures between 1 and −1 °C (Lotter et al., 2012; Eicher, 1995) and July temperatures between 9 and 11 °C (Bolland et al., 2020). This time is referred to as the Heinrich Stadial 1 (HS1) (> 18–14.6 ka cal BP). At ca. 14.6 ka cal BP, Dansgaard–Oeschger Event 1 (DOE-1) started with the Bølling warming, leading to an increase in annual temperature of 4–7 °C within a few decades (Eicher, 1995). The rapid warming at the onset of the Bølling was followed by a gradual cooling of ∼ 1.5 °C throughout the DOE-1 (Bølling/Allerød), which ended with the abrupt onset of the Younger Dryas (12.8–11.8 ka cal BP), with mean annual temperatures around 3 °C and July temperatures around 11 °C (Lotter et al., 2000).

3 Methods

3.1 Coring, lithology, and chronology

Parallel and overlapping sediment cores were taken from the basin bottom of Amsoldingersee in October 2022 using a UWITEC piston corer (46°43′30.9″ N, 07°34′34.3″ E;

Fig. 1c). A composite core AMS22-COMP1 was built from segments after stratigraphic correlation (Fig. S1 in the Supplement). The lithology was described according to Bos et al. (2012). Smear slides were compared to existing libraries (Myrbo et al., 2011).

The sediments were dated using ^{14}C dating, pollen biostratigraphy, and the Laacher See tephra (LST; Reinig et al., 2021). Consecutive 1 cm thick sediment samples were sieved (50, 100, and 200 µm mesh) to separate and taxonomically identify terrestrial plant macrofossils (Table S1 in the Supplement). Nine ^{14}C samples were prepared and measured with the MICADAS-AMS at the University of Bern (Szidat et al., 2014). Samples < 0.7 mg C were measured with direct gas injection. ^{14}C dates were calibrated using the IntCal20 calibration curve (Reimer et al., 2020). We combined ^{14}C dates with well-dated regional biostratigraphic markers by comparing pollen profiles in Amsoldingersee with those of Gerzensee and Moossee (Ammann et al., 2013; Rey et al., 2017, 2020). Previously reported ages for biostratigraphic markers (Table S1) were transferred to our core. Pollen was analysed in contiguous 2 cm intervals (Moore et al., 1991) up to the LST. Finally, the combined age–depth relationship was modelled using the Bacon package in RStudio (version 4.3.2) (Blaauw and Christen, 2011). The chronozones and their ages (Figs. 3, 5, 6, 8, and 9) are taken from Ammann et al. (2013).

3.2 Scanning XRF and hyperspectral imaging

XRF elemental composition was measured on clean surfaces of split cores using an ITRAX XRF core scanner at the University of Bern (5 mm resolution, 30 s integration time, Cr X-ray tube at 30 kV and 50 mA). For each core, triplicate scans (15 mm long) were taken at the top, middle, and bottom of the core to quantify and test the standard error of elements ($n = 27$). Raw data of Al, Si, K, Ti, Zr, Cu, Ca, Sr, Mn, Fe, and S had a relative standard error of < 15 % and were considered reproducible and thus used for further analysis. XRF data were summed and normalised to correct for matrix effects (Bertrand et al., 2023) and centred and log transformed (CLR) to correct for the closed-sum problem (Weltje and Tjallingii, 2008; Aitchison, 1982). XRF variables with near-zero counts can become extremely noisy after CLR; therefore, the CLR output of Zr and S was replaced with the minimum quantifiable value at intervals where the 10-point moving standard deviation was consistently larger than 0.5.

Hyperspectral imaging (HSI) offers a way to reconstruct primary production, hypolimnetic anoxia, and compositions of major primary producer groups at unprecedented (micrometre-scale) resolution on long timescales (Zander et al., 2023). Hyperspectral images were taken using a Specim PFD-CL-65-V10E line scan camera in the VNIR spectrum (400–1000 nm, 1.57 nm spectral resolution, 8 Hz, 120 ms exposure). Raw data are corrected with a white $BaSO_4$ and a dark standard. Data postprocessing follows Butz et al. (2015). Spectral troughs were identified from spectral endmembers, defined as pure pixels of minimal noise bands (dimensionally reduced dataset) (Butz et al., 2015). Relative absorption troughs were identified at 667, 844, and 619 nm. From these troughs, we calculate relative absorption band depth (RABD) values (Butz et al., 2015) using the formulas and interpretations in Zander et al. (2022):

- RABD667 is interpreted as the total green pigments (mostly chlorophyll and coloured diagenetic products, Tchl) and is a proxy for aquatic primary production.
- RABD844 traces the absorption of bacteriopheophytin *a* (Bphe *a*), a pigment produced by purple sulfur bacteria (PSB) that proliferate at the chemocline and are diagnostic of anoxia reaching the photic zone (Zander et al., 2021).
- RABD619 is related to phycocyanin (Wienhues and Zahajská et al., 2025), a pigment diagnostic of cyanobacteria.

RABD index values (Table S2) were calibrated to absolute pigment concentrations according to Butz et al. (2015), whereby concentrations of pigment extracts were measured using a Shimadzu UV-1800 UV–VIS spectrophotometer (Figs. S2 and S3). Extinction coefficients of Bphe *a* and Chl *a* in 90 % acetone are from Jeffrey and Humphrey (1975). The linear regression models were further evaluated with root mean square error of prediction (RMSEP), Cook's distance analysis, leverage plots, and tests of residual normality (Zander et al., 2022). The regression models are significant for RABD667 to Chl *a* ($r = 0.89$, $p < 0.001$, RMSEP $= 21.66\,\mu g\,g_{wet}^{-1}$ Chl *a*; 13.8 %) and RABD844 to Bphe *a* ($r = 0.83$, $p < 0.001$, RMSEP $= 6.34\,\mu g\,g_{wet}^{-1}$ Bphe *a*; 16.1 %). Currently, no method is available to calibrate the RABD619 index to phycocyanin (Wienhues and Zahajská et al., 2025). Our limit of quantification for RABD844 is $3\,\mu g\,g_{wet}^{-1}$ Bphe *a* and $5\,\mu g\,g_{wet}^{-1}$ Chl *a* for RABD667. Further details on the calibration are shown in Figs. S2 and S3.

3.3 TC, TN, and TS and sequential extraction of P, Mn, and Fe

We used CNS and sequential extraction of sedimentary P, Mn, and Fe to diagnose potential chemical feedback during events of hypolimnetic anoxia (Tu et al., 2021). A total of 5–8 mg of homogenised freeze-dried sediment was combusted in tin capsules to determine TC, TN, and TS with a FlashSmart™ 2000 NCS elemental analyser (Thermo Fisher Scientific). TOC was measured by combusting pre-acidified sediment in tin-packed silver capsules (Brodie et al., 2011). TIC was calculated as TC minus TOC. Detection limits were 0.01 % of dry sample weight for TC and TN and 0.05 % of dry sample weight for TS.

For the sequential extraction of P, Mn, and Fe, we used the extraction protocol of Lukkari et al. (2007) with 0.25 g

dry sediment to obtain five fractions of P, Mn, and Fe. Water content was calculated from the sediment weights before and after freeze-drying. P fractions were interpreted according to Lukkari et al. (2007), while Fe and Mn fractions were interpreted according to Scholtysik et al. (2022): F1 extraction with 0.46 M NaCl representing loosely bound, adsorbed, and porewater Mn, Fe, and P; F2 extraction with 0.11 M bicarbonate–dithionite (BD) yielding the reductive-soluble fraction of FeO_x, MnO_x, and P bound in these oxides; F3 extraction with 1 M NaOH yielding the rest of the P bound to Fe and Al oxides and organic P; F4 extraction with 0.5 M HCl targeting carbonate-bound Mn, Fe, and P; and F5 combustion at 550 °C and extraction with 1 M HCl for residual Mn, Fe, and P. A flowchart of the standardised operation protocol can be found in Lukkari et al. (2007). The sample and extractant volume ratio was always 1 : 200 (g : mL) (Lukkari et al., 2007). Extraction batches comprised 16 aliquots, 12 originals, 2 duplicate samples, 1 blank, and 1 reference (NIST2079a, San Joaquin soil). P, Fe, and Mn of all five fractions were measured using ICP-MS (Agilent Series 7600) in a 0.159 M HNO_3 matrix.

3.4 Analytical analysis of sedimentary pigments

Sedimentary pigments were used to investigate changes in past producer communities (Leavitt and Hodgson, 2001; Bianchi and Canuel, 2011). Pigments were extracted from $\sim$ 1 mL ($\sim$ 1.2 g) of wet bulk sediment following Lami et al. (2009). The sediment was suspended in 2.5 mL of 100 % high-performance liquid chromatography (HPLC)-grade acetone, vortexed (20 s), sonicated (1 min), centrifuged (3500 rpm, 10 min), and collected in an amber vial. Extraction steps were repeated until the extract looked colourless. The extract was filtered into a 1.5 mL HPLC vial (22 µm PTFE syringe filter) and kept dark and cold. Extracts were analysed with a Dionex Ultimate 3000 series (Thermo Fisher) high-performance liquid chromatography system with a diode array detector (DAD-3000RS) at 460 and 665 nm. Pigment separation was performed using reverse-phase chromatography employing a C18 column (Agilent Omnisphere 5) and a set of eluents following Lami et al. (2009) (Sect. S1 in the Supplement).

The chromatogram peaks were integrated into Chromeleon 7.2 (Thermo Fisher). Calibrations show that the chromatogram peak area scales linearly with the quantity of a substance; thus, integrated peak areas were calibrated to nanomole using predetermined HPLC-system-specific linear regression coefficients (Table S3). If no specific regression coefficients were available, we applied the linear relationships of β carotene to carotenoids and those of Chlorophyll a to green pigments. Most pigments discussed here were quantified by integrating Gaussian-fitted peaks on the chromatogram. Some exceptions are isorenieratene, car-52.58, lutein, zeaxanthin, α carotene, β carotene, and γ carotene, which overlap significantly. The peaks of these pigments were integrated using a perpendicular drop method (Westerberg, 1969), which results in a higher error.

We also used a non-target approach and named unknown carotenoids according to their retention times (e.g. car-21.2 elutes 21.2 min after injection). We classified green pigments more polar than Chl a as pheophorbides $x.x.x$, green pigments less polar than Chl a as pheophytins x, and green pigments less polar than β carotene as pyropheophytins x (Lami et al., 2009). We are aware that this classification may be incorrect in some cases. For example, pheophorbides between 30–45 min could also be bacteriochlorophyll c, d homologues (Romero-Viana et al., 2010).

Pigments were interpreted using the interpretation keys of Bianchi and Canuel (2011), Schlüter et al. (2006), and Lami et al. (2000) and the carotenoid database of Yabuzaki (2017) (Table S3). The chlorophyll preservation index (CPI), Chl a/(Chl a + pheophytin a), was used as an additional indicator of pigment preservation (Buchaca and Catalan, 2008). For some pigments, alternative interpretations have been found in the literature; in these cases, references are provided.

3.5 Statistical analyses

Data exploration was performed using principal component analysis (PCA). To differentiate between statistically different lithotypes, Ward's hierarchical clustering was applied to the high-resolution HSI and XRF data (cutoff at the Euclidean distance of 17); the lower-resolution P, Mn, and Fe; and the HPLC pigment datasets. As XRF data were centred and log transformed and HSI data were z scored, the data were normally distributed and could thus be compared in one plot. We verified PCA results and tested for non-linear dependencies by performing non-metric multidimensional scaling (NMDS) eliminate the "horse-shoe effect" in PCA (Podani and Miklós, 2002).

Carotenoids and green pigments were pre-selected using a threshold approach. Pigments not continuously present throughout the core (> 9 values of zero, $n = 59$) were excluded from further statistical analysis. Throughout the core, 44 carotenoids passed this threshold criterion. Carotenoids were grouped using Ward's hierarchical clustering on the correlation matrix of carotenoids (Kramer and Siegel, 2019). Subdivisions were created when subordinate patterns were observed in multiple pigment time series or when certain subgroups included diagnostic pigments with a specific ecological interpretation. CONISS clustering of the carotenoid dataset follows Grimm (1987); the number of significant clusters was determined using the broken-stick model.

We performed redundancy analysis (RDA; Legendre, 2012) and rate of change (RoC) analysis (Mottl et al., 2021) on the pigment dataset to determine which independent variables could explain the pigment variance and when the community significantly changed. For RDA (Fig. S9), we used the pollen record from Moossee (Fig. 1b, Rey et al.,

2020). To test whether anoxic phases had an irreversible effect on the algal community, we analysed the trajectories of the pigment community data in the eigenvalue space (second and third principal component scores). The MATLAB and R codes are available on GitHub (https://github.com/SJSchouten, last access: 30 July 2025).

4 Results and interpretation

4.1 Composite core and chronology

The composite core AMS22-COMP1 is 8.74 m long (Fig. S5). Basal gravel to sandy clastic sediment (8.74–7.65 m) is overlain by 2.65 m of laminated inorganic silty clay (7.65–5.56 m), followed by 5.56 m of gyttja (5.56–0.0 m). Here, we focus on the lower core sections 5.7–4.8 m, which span the Late Glacial and the transition to the Holocene.

The chronology (Fig. 2) is constrained by calibrated ^{14}C AMS ages of nine taxonomically identified terrestrial plant macrofossils (Table S1), three pollen-based biostratigraphic markers (Fig. S4), and the Laacher See tephra ($13\,006 \pm 9$ yr BP, Reinig et al., 2021), yielding ages between 14.9 and 10.5 ka cal BP, consistent between the different dating approaches. The modelled age uncertainty at 2σ ranges between 300 and 600 years. Despite continuous sediment sieving, no terrestrial macrofossils were found below 5.43 m sediment depth. Thus, the sediment section > 15 ka cal BP is constrained by the early regional *Betula* rise at $\sim 16 \pm 0.68$ ka cal BP (Rey et al., 2020). Accordingly, we estimate the age of the transition between silty clay and fine detrital gyttja (5.55 m sediment depth) to be ca. 16.2 ± 1 ka cal BP. Ages for the initial lake formation in this region date to < 19 ka cal BP (Rey et al., 2020), suggesting that 2.65 m of laminated silty clay at the bottom of the core was deposited in ca. 2–3 kyr, yielding a sediment accumulation rate (SAR) of > 1 mm yr^{-1} in the lower part of the core. The SAR between 16 and 10.5 ka cal BP was remarkably constant and an order of magnitude lower (0.11 mm yr^{-1}).

4.2 Lithology and sediment composition

Diagnostic inorganic and organic proxies, PCA time series, and Ward's hierarchical and CONISS-constrained clustering of all selected XRF and HSI proxies are displayed in Fig. 3. The complete XRF dataset is shown in the biplot of Figs. 4 and S5. Constrained and unconstrained clustering yielded similar results (six distinct clusters), suggesting that changes in the sediment composition (lithotypes) are predominantly stratigraphically constrained.

The PC1 axis (65 % of total variance; Fig. 4) separates organic sediment (aquatic primary production; positive) from lithoclastic sediments (erosion, runoff; negative). PC2 (21 % of variance) reflects redox and lake mixing conditions, whereby positive PC2 scores represent high Bphe *a* concentrations (well-stratified lake with hypolimnetic anoxia), and negative PC2 scores relate to well-mixed oxygenated conditions with sequestration of redox-sensitive metals such as Mn and Cu. The PCA shows signs of non-linear dependency (horseshoe effect). Therefore, we performed standardised euclidian MDS (Fig. S6), already yielding a decent fit with just one component (at a stress of 0.14). On the two-component MDS (stress of 0.06), we performed Ward's clustering, which annotated clusters similar to those of the PCA; thus, we conclude that our PCA-derived clusters are robust.

Unconstrained clustering of the high-resolution dataset (XRF and HSI) revealed six lithotypes (LTs).

Lithotype 1 (LT 1; 5.70–5.56 m, $\sim 18/\sim 16.2$ ka cal BP; Heinrich Event 1, H1) is a light grey (7.5YR5/1 Munsell), homogenous inorganic (0.4 % C_{org} and 21 % water content) detrital carbonaceous silty clay that contains no plant macrofossils or diatoms and is poorly sorted, with most grains being sub-rounded to rounded. The lithotype is elevated in Ca, Sr, Fe, Si, Ti, and TIC (4.5 %–6 %) and is interpreted as having high accumulation rates of fine clastic sediments. Total pigment concentrations, indicative of primary production (PP), are very low (Tchl in Fig. 3). We interpret this lithotype as eroded glacial till washed into a young oligotrophic perennial lake.

Lithotype 2 (5.56–5.51 m, ~ 16.2–15.8 ka cal BP, H1) is a light brown (10YR4/1 Munsell), heterogenous organic (3.5 %. C_{org} and 46 % water content) silty clay that contains no plant macrofossils or diatoms and angular to rounded grains. It is elevated in Fe, Ti, and Si. TIC (1 %), Ca, and Sr decrease rapidly (Fig. 3). The sediments are enriched in S, and C/N ratios < 10 suggest a predominantly aquatic origin of the organic matter (Meyers, 1997). The increase in aquatic PP is marked by a moderate increase in green pigments (Tchl), an increase in phycocyanin (cyanobacteria), and high amounts of Bphe *a*, suggesting a chemocline in the photic zone and hypolimnetic anoxia. This lithotype is interpreted as having a predominantly clastic lacustrine deposition in a stable deglacial landscape with widespread lake stratification and anoxia, oligotrophic conditions, and lower SAR during H1 (Oldest Dryas).

Lithotype 3 (5.51–5.38 m, 15.8–14.7 ka cal BP, H1) is a light brown (10YR3/2), laminated (1–10 mm) heterogenous detrital gyttja (3.5 %–8.5 % C_{org} and 48 %–60 % water content, 0.1 %–1.5 % TIC) with sparse plant macrofossils and diatoms and subangular grains. The organic matter content fluctuates with the sediment brightness. Inorganic laminae contain more clastic sediments with sharp contacts and darkening upward (elevated Ca, Sr, Ti, Fe, and Si). Organic laminae contain higher concentrations of CNS, Tchl, and phycocyanin; C/N values are < 10 (Fig. 3). Bphe *a* concentrations lie around the detection limit, except for a distinct local peak around 5.44 m. Generally, LT 3 is relatively enriched in Ti, Zr, and Fe and depleted in Ca, Sr, and TIC (top-left quadrant in the PCA, Fig. 4), suggesting that there is a source of siliciclastic sediment that comes from outside the carbonate-

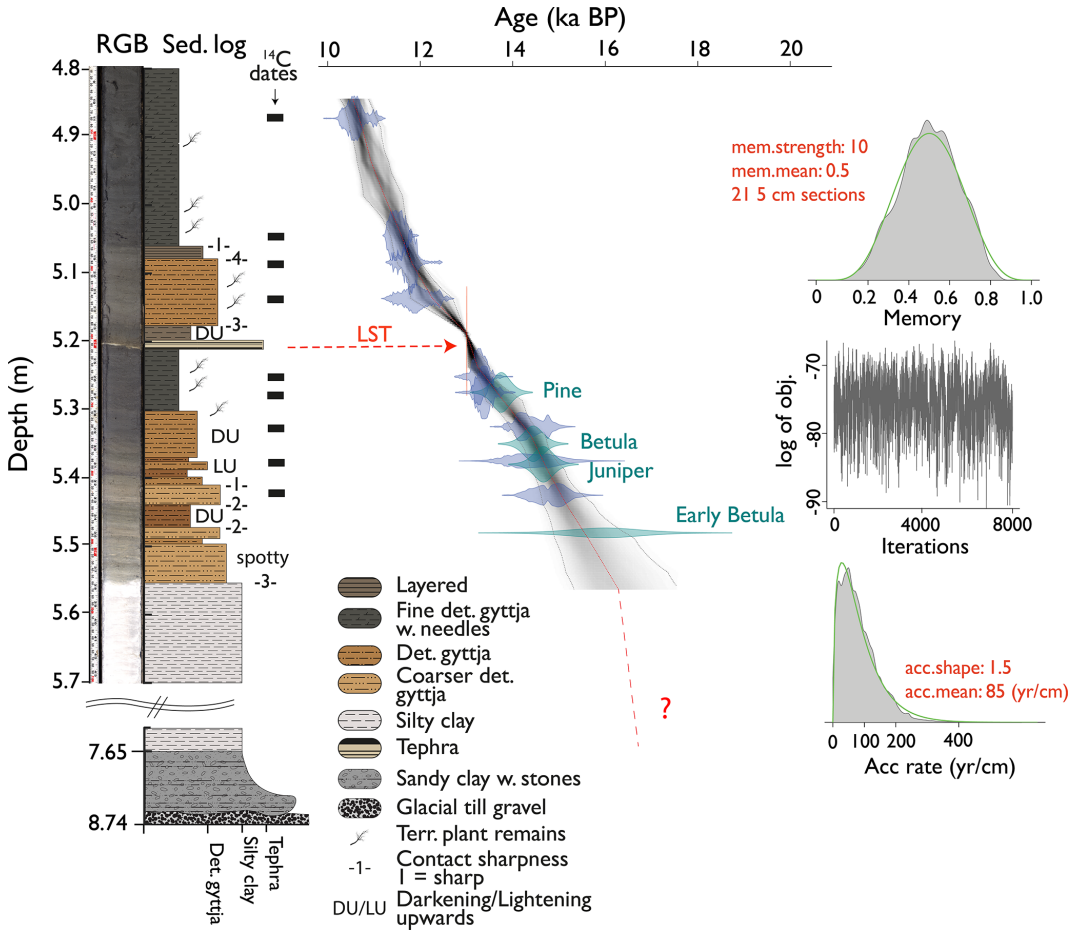

Figure 2. True-colour RGB picture and lithology (left) and age–depth relationship of the composite core AMS22-COMP1 (right) of Late Glacial Amsoldingersee sediments. The green violin plots indicate biostratigraphic tie points, whereas the blue violins indicate the distribution of ^{14}C age probabilities. The LST is marked in red. Priors to the Bayesian run are plotted on the right side.

dominated catchment. We interpret sediments of LT 3 (the latest part of H1) as lacustrine deposits in a deglacial landscape, with reduced erosional influx (lower Ca and TIC), increasing aquatic PP, and traces of airborne dust (high Ti and Zr).

Lithotype 4 (LT 4; 5.38–5.18 and 5.09–5.05 m, 14.7–12.9 and 11.9–11.7 ka cal BP, respectively; Bølling/Allerød (B/A) except LST and the last part of the Younger Dryas, YD) is a dark brown (10YR3/2 Munsell), homogeneous organic detrital gyttja (15 %–28 % C_{org} and 72 %–80 % water content, 0.5 % TIC) with *Betula* macrofossils, sparse diatoms, and rounded grains. LT 4 has low Ti, Fe, and Si and high S and Mn values (Fig. 3). C/N ratios are higher than before and range between 10 and 11. Tchl (aquatic PP), $Cr_{coh}Cr_{incoh}^{-1}$, and PC1 are moderately high. Bphe *a* (PSB, anoxia) concentrations are variable, with local peaks at around 5.31 and 5.24 m. Phycocyanin is constantly present, reaches a maximum at 5.23 m, and remains high afterwards. In the upper section of LT 4 (5.09–5.05 m), all pigment concentrations decrease, and Bphe *a* gets close to the limit of quantification. We interpret sediments of the lower part of LT 4 (B/A) as deposits in a stable landscape with relatively lower clastic influx and relatively higher aquatic PP. The lake was well mixed, with poor development of hypolimnetic anoxia, except for two episodes at around 5.30 and 5.22 m sediment depth. The sediments of the upper part of LT 4 (end of YD) are interpreted as deposits in a cold and dry environment with allochthonous clastic influx and low lake levels.

Lithotype 5 (LT 5; 5.21–5.19 and 5.18–5.09 m, 13.0–11.9 ka cal BP; LST and Younger Dryas) is a brown (10YR2/2 Munsell), homogeneous detrital gyttja with slightly lower OM concentrations than in LT 4 (15 %–25 % C_{org} and 71 %–78 % water content), abundant diatoms, and *Pinus* and *Betula* macrofossils. Grains are mostly subrounded and poorly sorted, and the lithotype contains low Ca, Sr, and TIC (0.7 %) but elevated Ti, Fe, Si, K, Zr, and S values (Fig. 3). This suggests that, very similar to LT 2 and LT 3 (PC2 positive, Fig. 4), the clastic sediment fraction bears a significant proportion of allochthonous sources, potentially airborne mineral dust. In contrast, erosion of car-

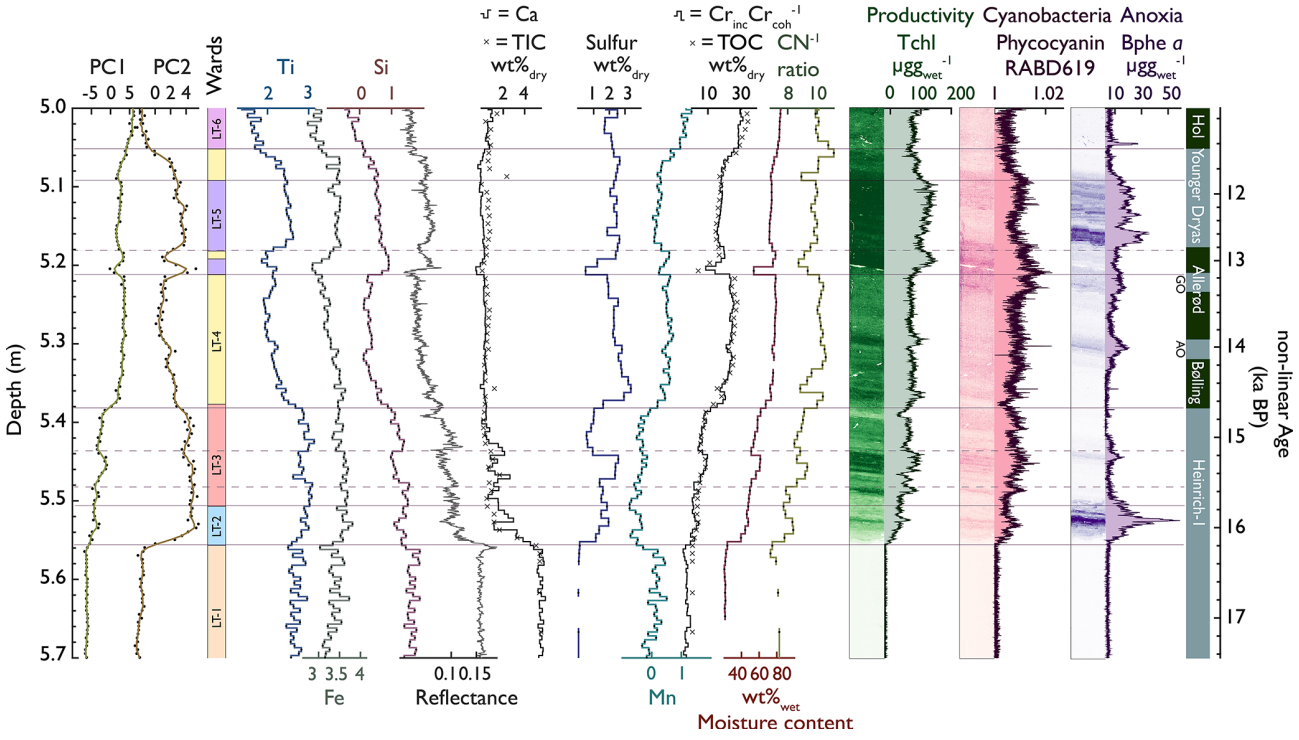

Figure 3. PC1 and PC2 values (data from Fig. 4), Ward's hierarchical unconstrained and CONISS-constrained clustering (horizontal lines), and selected biogeochemical proxies. The hyperspectral data (right) are plotted as intensity maps and time series. The colours of the lithotypes (LTs) are the same as in Fig. 4.

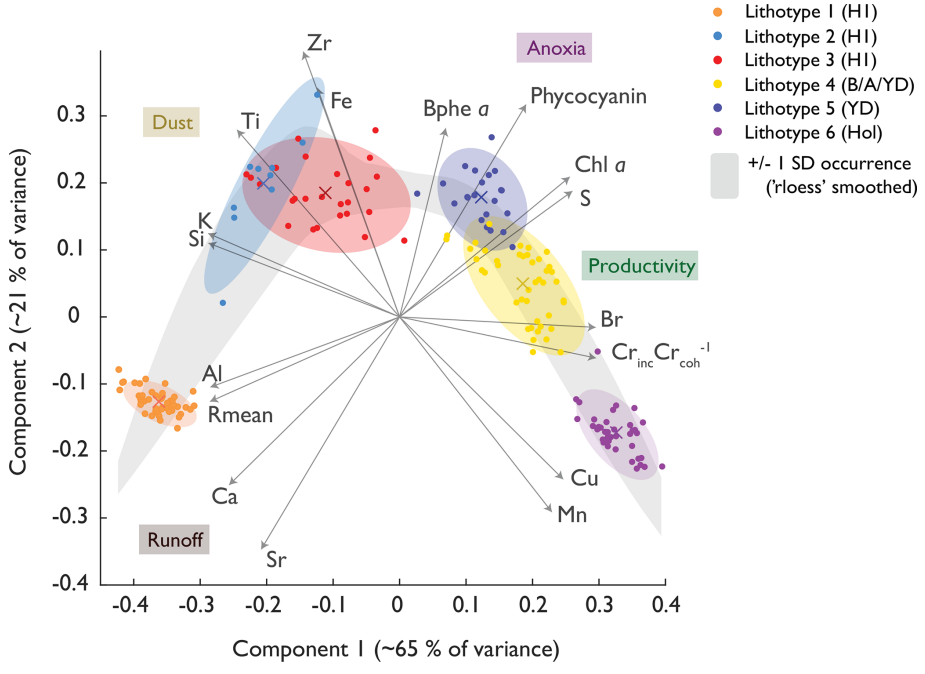

Figure 4. Principal component plot of the XRF and HSI proxies. Ward's clusters are coloured along their confidence ellipses. The grey band indicates a smoothed depiction of the standard deviation of the PC1 and PC2 data, providing a band of "common occurrence". The environmental interpretation of the PCs is indicated in coloured boxes.

bonates from the catchment remained limited. S concentrations remain high, which is different from the inorganic LT 2. Phycocyanin is generally high and reaches two maxima (5.21–5.18 and 5.14–5.10 m). Bphe *a* (PSB, anoxia) and Tchl (aquatic PP) values are the highest throughout LT 5. We interpret both sections of LT 5 as lacustrine sediments formed in a dry (low surface erosion in the catchment) and cold environment with high dust or tephra loads, hypolimnetic anoxia, and high aquatic PP.

Lithotype 6 (LT 6; 5.05–4.8 m, 11.7–11.3 ka cal BP; early Holocene) is a dark brown (10YR2/1 Munsell), highly organic homogenous detrital gyttja (30 %–35 % C_{org} and 81 %–85 % water content, 1 % TIC) with reduced lithoclastics (Fig. 3). This unit contains large terrestrial macrofossils, diatoms, and sparse sub-rounded to rounded grains. C/N ratios are relatively high and range from 10 to 11, comparable to LT 4; Tchl (aquatic PP) and phycocyanin (cyanobacteria) remain at levels similar to LT 4 (B/A). Bphe *a* values are below the limit of quantification, suggesting that the lake was well mixed. LT 6 (early Holocene) was deposited in a stable environment with very low lithoclastic input and high aquatic PP.

4.3 Fractions of P, Mn, and Fe

CONISS and Ward's clustering of Fe, Mn, and P fractions revealed four significant clusters (Figs. 5 and S7) with two transitions that align with the lithotype changes (end of LT 1 and end of LT 2). The transition from Cluster 3 to Cluster 4 suggests a change in the P, Mn, and Fe fractions during the Younger Dryas. The four clusters are ordered along PC1 (48 % of total variance), which ranges from residual (lithogenic) fractions (PC1 negative) to organic fractions (PC1 positive), and PC2 (19 % of total variance), which reflects redox conditions (anoxia, PC2 positive). The trajectories (Fig. S7, grey arrows) display a trend from catchment processes (16–15 ka cal BP) with Ca-bound and residual P (F4 and F5); Fe and Mn oxides, oxyhydroxides, and carbonates (F4); and residual Fe and Mn (F5) towards organic-bound fractions (F3, 14–13 ka cal BP) and elevated redox-sensitive fractions (13–11 ka cal BP).

Total phosphorous is relatively stable throughout the record ($520 \pm 94\,\mu g\,g_{dry}^{-1}$). Ca-bound phosphorous (P–F4) is the dominant fraction, ranging from 31 %–89 % (mean = 63 %) in the lower and upper parts of the core (below 5.37 m and above 5.18 m, corresponding to H1 and YD, respectively), whereas the Ca–P fraction is relatively small (28 %–55 %) in the middle part of the core (B/A). Interestingly, Ca–P covaries, with elements attributed to allochthonous siliciclastics from atmospheric dust (Fig. 3b, like Ti $r^2 = 0.92$, $p < 0.001$), and correlates less with elements interpreted as clastic sediments from local runoff like Ca ($r^2 = 0.54$, $p < 0.001$), suggesting that significant proportions of Ca–P and thus P are related to allochthonous inorganic dust deposition during cold periods (H1 and YD). The fraction of residual phosphorous (P-F5) is relatively small (mean = 17 %) and stable throughout the record.

During the Bølling/Allerød (5.37–5.18 m), P_{org} (F3) covaries with sediment organic matter TOC ($r^2 = 0.7$, $p < 0.001$). Redox-sensitive P (P-F2) was undetectable in almost all samples throughout the record, suggesting that bioavailable P was minimal and, if present at all, constantly internally recycled, particularly during anoxic periods.

In contrast to P, total Mn varies between 100 and $900\,\mu g\,g_{dry}^{-1}$. Residual Mn is generally low (13–61 $\mu g\,g_{dry}^{-1}$) and covaries with Ti and Zr. Ca-bound Mn (Mn-F4) and redox-sensitive Mn (Mn-F2) have the largest variability. Carbonate-bound Mn occurred in the silty clay of LT 1 and the LST. TIC (carbonate), Ca, Sr, and Mn and Fe carbonates have a similar downcore distribution and likely have a common origin. Porewater and organic Mn and Fe (Mn-F1, Fe-F1, and Mn-F3, as well as Fe-F3) occurred in the most organic sections of the record (LT 3 and LT 4: 5.37–5.05 m) and covary with $Cr_{inc}Cr_{coh}^{-1}$ and TOC.

The redox-sensitive fraction of Mn was abundant during the H1 and YD phases (< 5.37 and 518–5.05 m). Under conditions of hypolimnetic anoxia (high Bphe *a*), redox-sensitive Mn (Mn-F2) decreased, suggesting partly reductive dissolution and recycling. Residual Fe-F5 is more abundant than Mn-F5 and is mostly elevated during the H1 and Younger Dryas phases (< 5.37 cm and 5.18–5.05 m). F4 and total iron concentrations were more stable (800–$1800\,\mu g\,g_{dry}^{-1}$).

4.4 Pigment stratigraphy

We identified four significant carotenoid groups (Fig. 6). In Group 1, anoxygenic phototrophic bacteria (APB) peak during the early phases of H1, the Older Dryas, and the Younger Dryas. In Group 2, APB, diatoms, and other silicifiers peak during H1 and the YD. In Group 3, purple non-sulfur bacteria, green algae, dinoflagellates, and euglenids follow annual temperatures and peak in the Bølling. In Group 4, mainly cryptophytes and cyanobacteria are constantly high throughout the Bølling, Allerød, and YD.

CONISS clustering revealed five pigment zones (PZ, Fig. 6) which correspond well to the lithotypes (summarised in Fig. 8). These were also the phases of significant changes in algal composition, as highlighted by RoC analysis (Fig. 8): RoC maxima occurred after the LST at the transition to the YD, suggesting that these two events had the largest impact on primary producer communities. Further phases of statistically insignificant change happened mainly during Heinrich 1 and during periods of rapid warming (onsets of the Bølling and Holocene).

Pigment zone 1 (PZ 1) (below 5.56 m; < 16.1 ka cal BP, corresponding to LT 1) contains low amounts of pigments, primarily representing diatoms (Group 2.2) and APB (Group 1), suggesting oligotrophic conditions in a young deglacial landscape (Fig. 6).

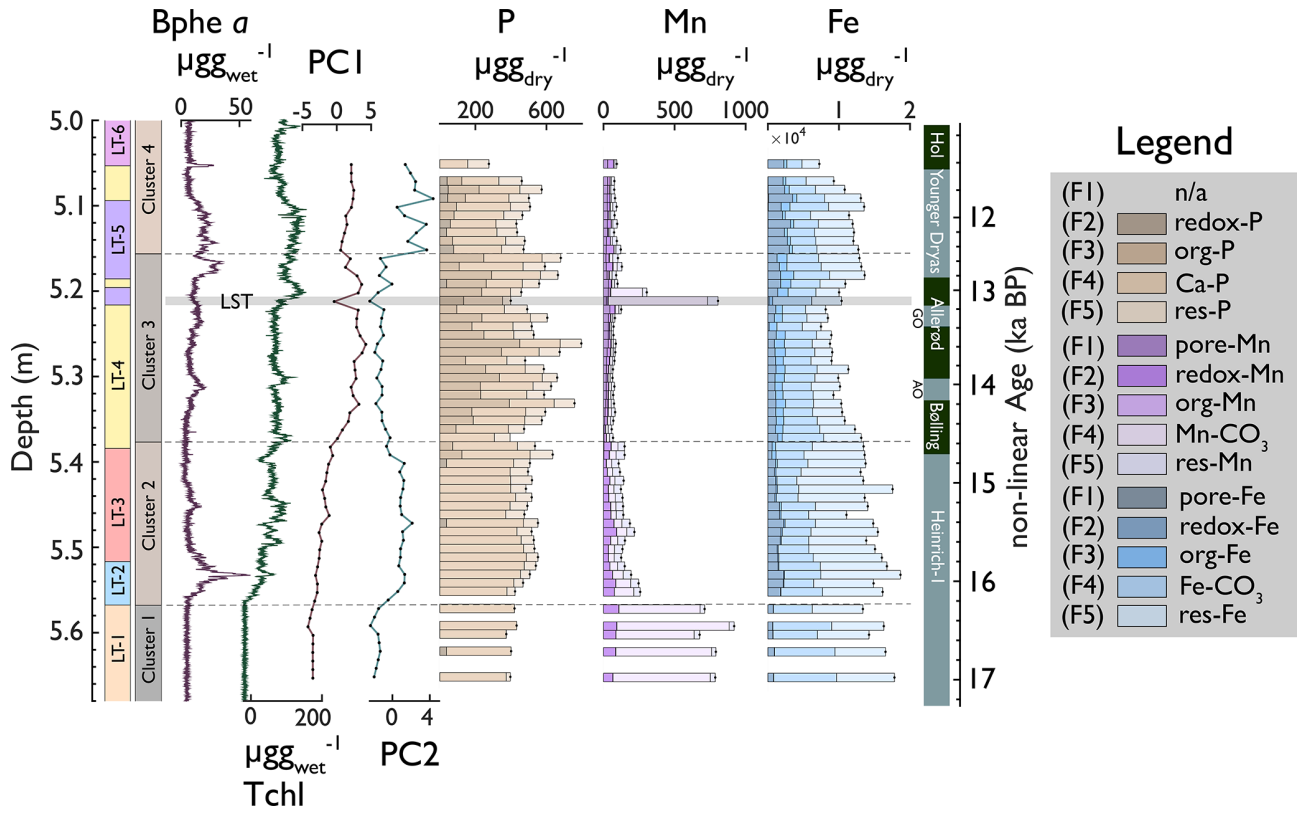

Figure 5. Downcore stacked bar plots of P, Mn, and Fe fractions; PC1 and PC2; and Clusters 1–4 of P, Mn, and Fe fractions (data from Fig. S7). Hyperspectral proxies and lithotypes are shown for orientation on the left. The darker colours indicate the redox-sensitive and readily dissolvable fractions of P, Mn, and Fe.

PZ 2 (5.56–5.38 m; 16.1–14.7 ka cal BP, corresponding to LT 2 and LT 3) marks an increase in aquatic production (chlorophyll and carotenoids) and shows a pigment succession with three phases (PZs 2a, b, and c, Fig. 6): initially, APB (Group 1) dominate with admixtures of carotenoids related to diatoms and other silicifiers (Group 2) and traces of cyanobacteria (Group 4.3). This pigment assemblage suggests intense and prolonged lake stratification or even meromixis with a chemocline in the photic zone. A minor anoxic phase is also observed later in PZ 2 at around 5.45 m (15.2 ka cal BP). Subsequently (5.49–5.44 m; PZ 2b), the APB community (Group 1) mostly disappears and is replaced by purple non-sulfur bacteria (PNSB) (Group 3.1), green algae (Group 3.2), and some cyanobacteria (Group 4.3). PZ 2 ends with a relative decrease in total carotenoids (Fig. 6), except for some nutrient-stress-related carotenoids of green algae (Group 4.1); this phase has a low chlorophyll preservation index (CPI), suggesting pigment degradation related to high water clarity and/or shallower water.

PZ 3 (5.38–5.21 m; 14.7–13.1 ka cal BP, corresponding to LT 4) shows a further increase in aquatic PP (total chlorophyll and diagenetic products, total carotenoids). Pigment assemblages are generally diverse (Fig. 6), representing PNSB, green algae, euglenids, (stressed) green algae (Table S3), cryptophytes, and cyanobacteria (Groups 3 and 4). Except for the short anoxia event at 5.32 m, APB are hardly present (Groups 1 and 2.1). At the onset of PZ 3 (5.38 m; 14.7 ka cal BP, start of Bølling warming), we observe a second succession (PZ 3a; Fig. 6) from astaxanthin (Group 4.1) to chloroxanthin (Group 3.1), then to diatoxanthin (Group 2.2), followed by lutein (Group 3.2) and echinenone (Group 4.3). This suggests a successive shift from nutrient-stressed growing conditions via nutrient fixing to more favourable growing conditions with abundant pigments and high pigment diversity (PZ 3b). This succession takes ca. 800 years after the onset of the warming. During and after this succession, pheophorbide *a* concentrations increase (absolute and relative to Chlorophyll *a*), suggesting simultaneous zooplankton grazing (Table S3). Towards the end of PZ 3 (PZ 3c), a relatively minor community shift occurs from green algae towards more cyanobacteria. PZ 3 ends with the LST.

PZ 4 (5.20–5.10 m; 13.07–11.90 ka cal BP, corresponding to LT 4 and LT 5) spans the late Allerød and the early YD. Immediately after the LST, the community is dominated by diatoms, other silicifiers, and cryptophytes/dinoflagellates (Groups 2.2 and 4.2, Fig. 6), suggesting silica fertilisation through tephra deposition. Tchl (HSI) and total carotenoids

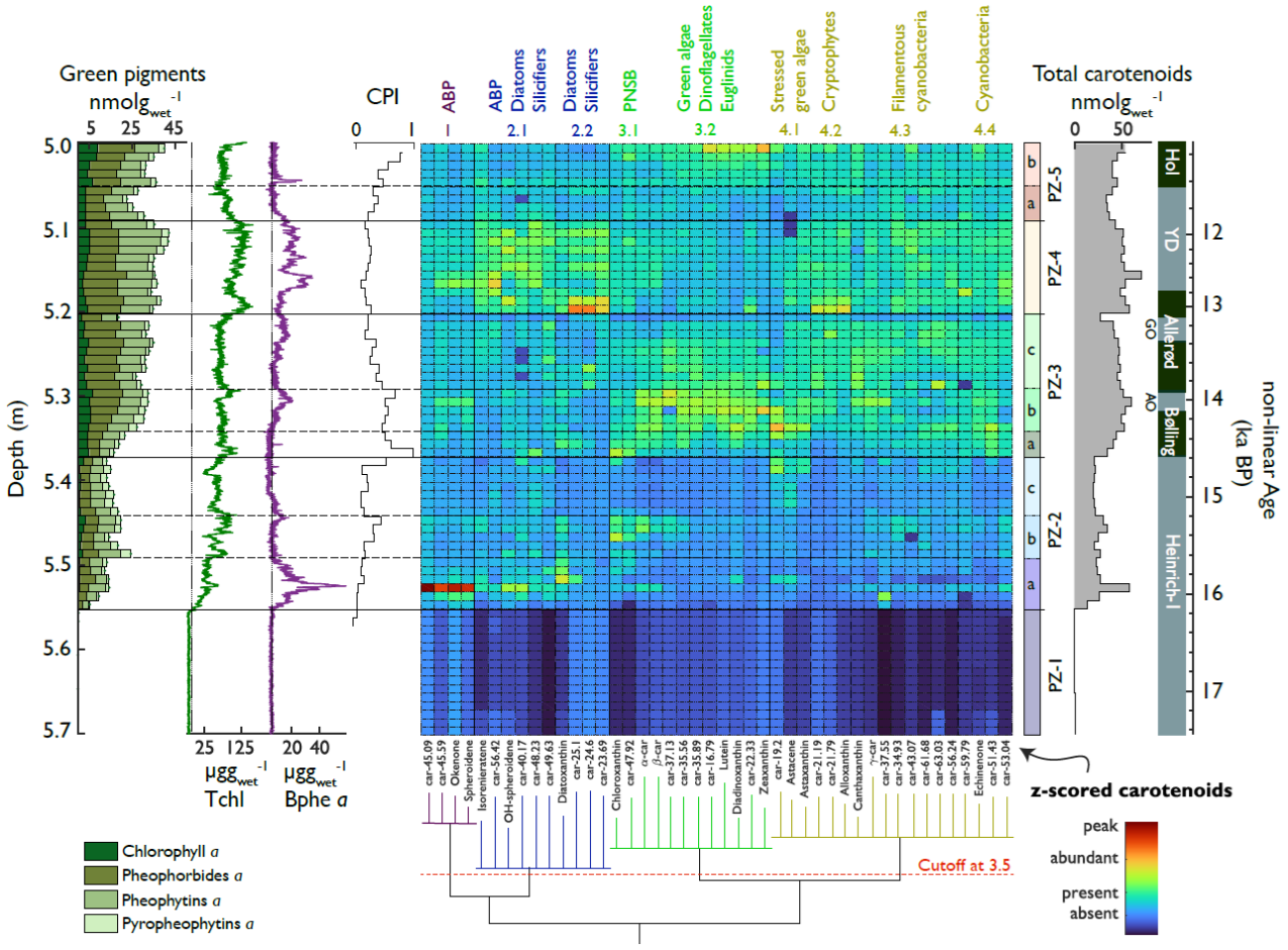

Figure 6. Downcore concentrations of pigments and HSI, together with a heatmap of grouped carotenoids. Left: sums of Chl *a* and diagenetic products (stacked bar graph), HSI indices (for orientation), and CPI. Middle: heatmap of the *z* scores of carotenoids ordered with respect to their statistical correlation into four carotenoid groups (bottom dendrogram) with subdivisions. Right: pigment zones derived from CONISS clustering with subzones (arbitrary, horizontal dashed lines) and total carotenoid sums (shaded). Pigment concentrations are shown in Fig. S8.

reach maximum levels. Our data show that the tephra fertilisation effect lasted several decades. Diatoms and cryptophytes remain abundant in the second part of PZ 4 (corresponding to the YD) (Groups 2.2 and 4.2). Bphe *a* (APB) and carotenoids related to anoxygenic bacteria (Groups 1 and 2.1) return, suggesting strong lake stratification, prolonged hypolimnetic anoxia, and a chemocline in the photic zone. PZ 4 also includes many pigments typically produced by (filamentous) cyanobacteria (Groups 4.2, 4.3, and 4.4).

PZ 5 (5.10–5.01 m, 11.90–11.32 ka cal BP) corresponds to the end of the YD (LT 4) and the early Holocene (LT 6). During the end of the YD (PZ 5a), all pigment concentrations are relatively low (Fig. 6) and primarily represent cyanobacteria (Group 4.3), non-sulfur bacteria (Group 3.1), and diatoms (Group 2.1). This drop corresponds to a phase with low CPI values and is possibly linked to enhanced uniform photodegradation. PZ 5b corresponds to the onset of the Holocene, with higher aquatic production dominated by green algae and subordinate cryptophytes, cyanobacteria, and purple non-sulfur bacteria. Group 3.2 gains immediate dominance following the abrupt Holocene warming. The lack of algal succession suggests that nutrient constraints were less critical at the Holocene's onset than at the Bølling's onset. After the onset of the Holocene, pigments are better preserved (increasing CPI).

To observe pigment composition in multivariate space, all extracted pigments (carotenoids and photopigments) are displayed as variables to their second and third principal components in Fig. 7a. PC2 (9 % of the variance) and PC3 (7 % of the variance) discriminate between taxonomic and ecological communities, which is of interest here. In comparison, PC1 (63 % of the variance, Fig. S10) follows total aquatic primary production, and PC2 separates pigments produced in the epilimnion during stratified conditions (anoxic hypolimnion) and cold and dusty phases (positive) from pigments produced during well-mixed, oxic, warm, and nutrient-limited phases

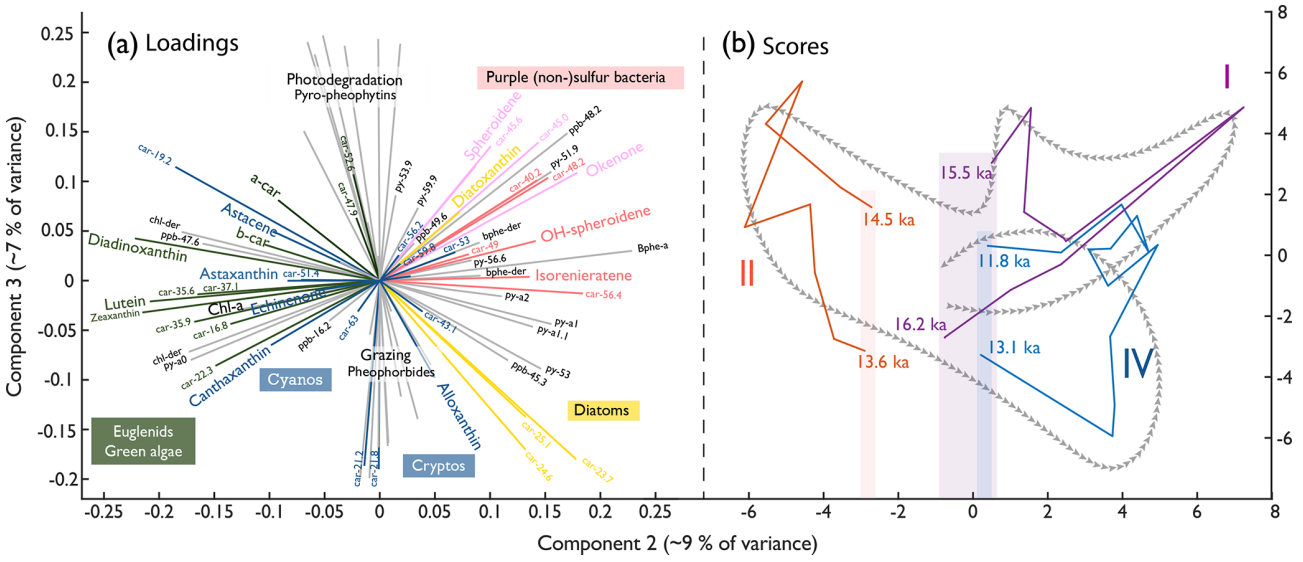

Figure 7. Principal component loadings (left) separating the algal communities and score trajectories (right) of all extractable pigments. **(a)** PC2 and PC3 of the pigment data. Carotenoids are coloured according to their statistical grouping (Fig. 6). Photopigments: ppb, pheophorbides; ppy, pyropheophytins; py, pheophytins. **(b)** Trajectories of the PC2 (9 % of variance) and PC3 (7 % of variance) scores throughout the three major anoxic phases (I, II, and IV; Fig. 8). The shading indicates the starting and ending point range of the individual anoxic phases along PC2. The grey arrows indicate a schematic of the overall trajectory during the Late Glacial, e.g. the same as for I, II, and IV but then covering the whole record.

(negative). PC3 separates (pyro-)pheophytins, which indicate photodegradation of chlorophyll, from pheophorbides, indicating enzymatic breakdown of chlorophyll, including zooplankton grazing in the epilimnion, essentially separating degradation pathways (Bianchi and Canuel, 2011; Lami et al., 2000). PC3 also provides a distinction between diatoms and PSB. Clustered pigments matching the carotenoid groups are likely produced by the same organisms or in similar environments. Four non-bacterial photopigments (ppb-48.2, py-51.9, py-59.9, and ppb-49.6) occur in the quadrant with anoxic carotenoids. These substances could be homologues of bacteriochlorophyll *b*, *c*, *d*, and *f* (Romero-Viana et al., 2010) produced by green-pigment-producing APB.

We analysed pigment PCA scores (PC2 and PC3) in a trajectory plot (Fig. 7b) to test if Late Glacial anoxia invoked irreversible changes in algal composition. Anoxygenic phototrophs dominate the initial algal community. The community develops towards green algae and cyanobacteria during the B/A interstadial, transitions to diatoms during the YD, and – finally – ends close to the starting point, suggesting that the overall Late Glacial trajectory (dashed arrow) left no irreversible compositional imprint. Moreover, the trajectories through the three main individual anoxic phases (Figs. 7b and 8, purple, red, and blue) returned to a comparable state concerning PC2 (taxonomy and ecology). In contrast, individual anoxia trajectories ended up with different PC3 values (degree of degradation), suggesting that, at the end of anoxia event 2, grazing pressure was higher than at the beginning, whereas for anoxic phases 1 and 4, grazing pressure seemed to be lower.

5 Discussion

5.1 Late Glacial lake evolution in the context of climatic and environmental conditions

In Amsoldingersee, sediment composition reflects aquatic organic matter vs. inorganic matter (PC1 axis, Fig. 4) and two different sources of clastic material, aeolian dust and runoff, from the catchment (PC2, Fig. 4). Pigment assemblages are influenced by temperature, lake stratification, oxygen availability, nutrients, and degradation processes. In our core (AMS22-COMP1), the lithotypes and pigment zones align stratigraphically (Fig. 8), suggesting that the processes controlling sediment composition and pigment assemblages have a common driver.

Earlier studies from nearby Gerzensee (Eicher, 1987) and other Swiss sites (Lotter et al., 1992) show that environmental changes on the Swiss Plateau responded very closely to large-scale climatic shifts in the North Atlantic domain during the Late Glacial (Ammann et al., 2013; van Raden et al., 2013). To place our findings in the context of the large-scale Late Glacial palaeoclimate evolution, we discuss the development of Amsoldingersee along chronozones (Ammann et al., 2013).

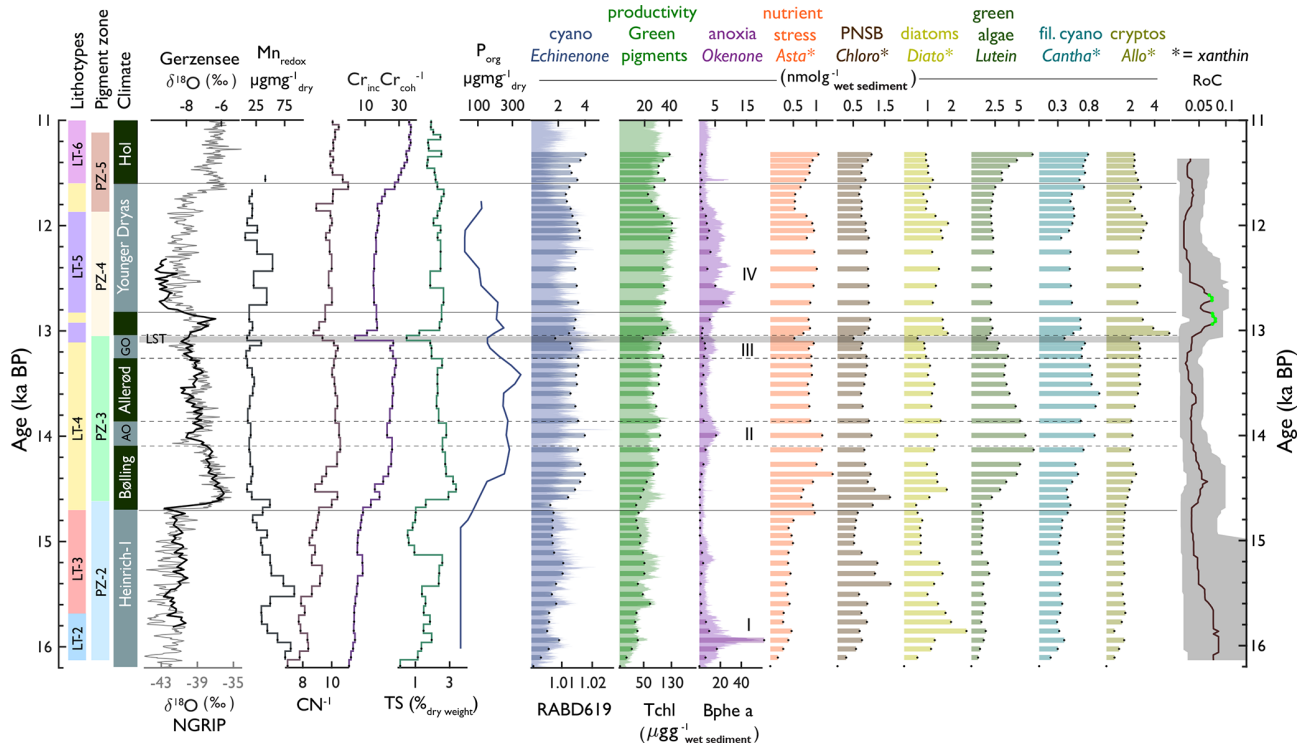

Figure 8. Compilation of lithotypes, pigment zones, chronostratigraphic zones (with $\delta^{18}O$ of Gerzensee and NGRIP to illustrate temperature, Ammann et al., 2013), selected geochemical proxies (Mn_{redox}, C/N, $Cr_{coh}Cr_{incoh}^{-1}$, TS, and P), selected pigments, and rate of change (of HPLC pigments).

5.1.1 Heinrich Stadial 1 (H1; ∼18–14.69 ka BP)

Amsoldingersee formed during H1, when retreating glaciers left a depression in the drumlin landscape (Fig. 1a). The sediment record starts with 2.65 m of laminated calcareous silty clay deposited into an early-deglacial oligotrophic perennial lake. Around 16.2 ka cal BP, the sediment composition shifts to an organic gyttja. This transition marks an abrupt end to silty clay input into the Amsoldingersee Basin. The sharp lithological transition can be explained as a decrease in sedimentation rates accompanied by increased organic matter deposition and a substantial reduction in detrital clastic input, suggesting increased landscape stability. No changes in local vegetation composition are observed, and our data are insufficient to conclude on the cause of this lithological change.

During H1, starting at 16.2 ka cal BP (Fig. 7), anoxygenic phototrophic bacteria (APB) and some cyanobacteria inhabited the lake, indicating hypolimnetic anoxia during the very early phase of the lake development. APB have an advantage over other photosynthetic organisms in light-limited conditions (Karr et al., 2003). In Amsoldingersee, light could have been limited because of suspended solids in deglacial windy environments and/or prolonged winter ice cover. Our results confirm earlier findings of pre-Bølling anoxia in Lobsigersee (Züllig, 1986). Indeed, long ice cover favours lake stratification and anoxia (Klanten et al., 2023), even in oligotrophic conditions.

Around 15.6 ka cal BP and onward, aquatic PP increased (TChl, Fig. 9b). Summer season temperatures warmed by about 2 °C, as reported for the greater Swiss Plateau (Rey et al., 2020; Bolland et al., 2020; Fig. 9h). This warming is not found in the $\delta^{18}O$ NGRIP record. Apparently, the summer warming around 15.8 ka cal BP initiated a simultaneous increase in terrestrial (*Betula*, Fig. 9c; Rey et al., 2020) and aquatic production (mainly green algae and cyanobacteria, as well as lutein and echinenone).

While this regional summer warming persisted (Bolland et al., 2020), aquatic PP dropped in Amsoldingersee after 15.1 ka cal BP (Fig. 9b), and dust input increased slightly (Ti, Fig. 9g). A trend towards less negative $\delta^{18}O$ values from the nearby Sieben Hängste speleothem (Fig. 9f) has been interpreted as strengthened northerly winds during that time (Luetscher et al., 2015). The CPI is low, and pyropheophytins are relatively abundant, suggesting extensive photodegradation of pigments (Buchaca and Catalan, 2008). Persistent drought and low lake levels could explain photodegradation during a cold phase within H1. Glacial readvances were documented in the Swiss Alps during that time (Daun, Clavadel/Senders, Ivy-Ochs et al., 2006).

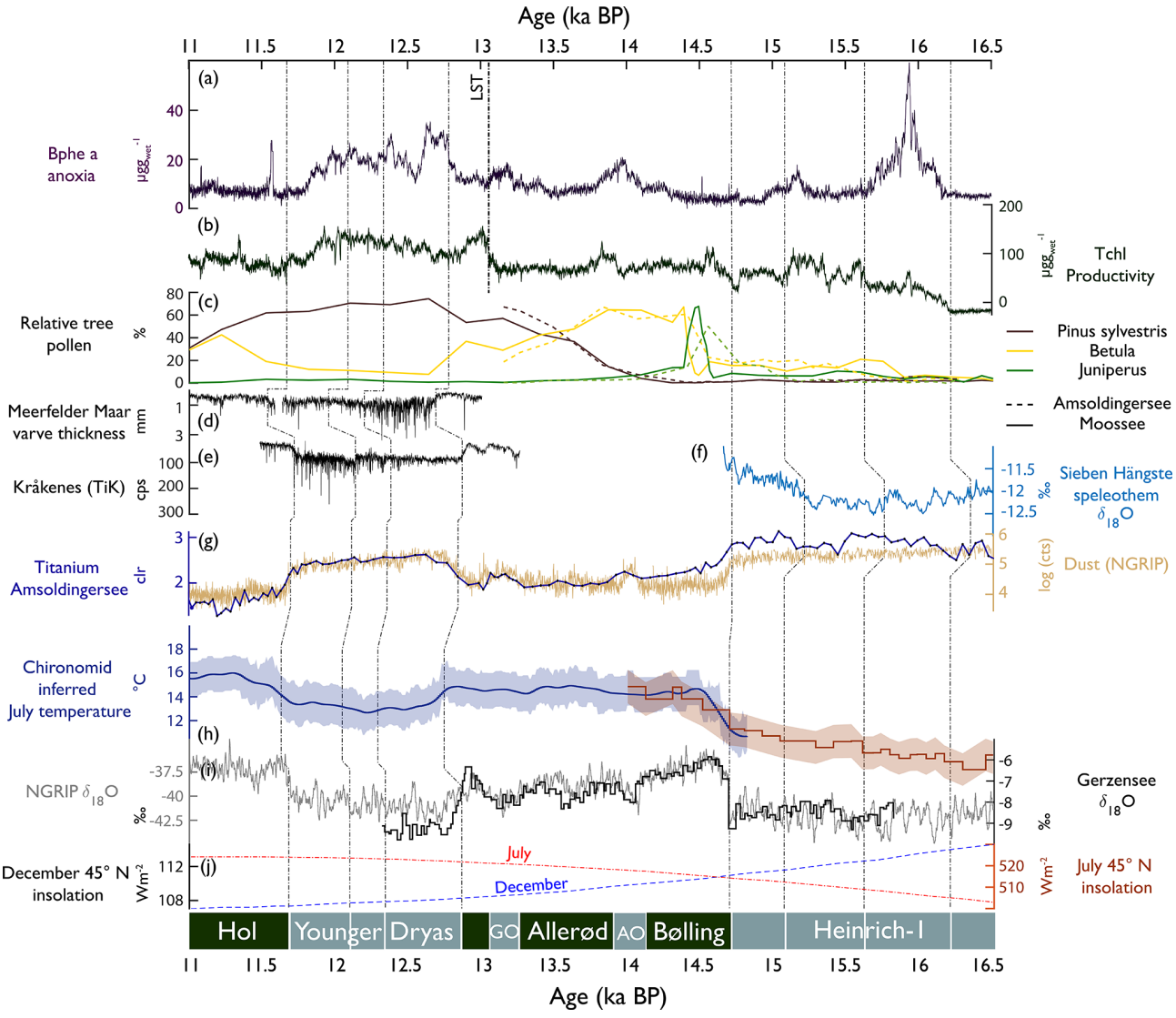

Figure 9. Comparison of proxy time series from Amsoldingersee (this study) with sites in the North Atlantic/European domain between 16.5 and 11 ka cal BP. **(a)** Bphe *a*, anoxia (this study); **(b)** Tchl, primary production (this study); **(c)** pollen records from Amsoldingersee (this study) and Moossee (Rey et al., 2020); **(d)** Meerfelder maar varve thickness (Brauer et al., 2008); **(e)** Kråkenes TiK representing runoff (Bakke et al., 2009); **(f)** Sieben Hängste speleothem δ^{18}O, with higher values representing more northerly flow (Luetscher et al., 2015); **(g)** log of NGRIP dust counts and Ti abundance (this study); **(h)** smoothed chironomid-inferred July temperature from the Alpine stack (blue, Heiri et al., 2015) and Burgäschisee (red, Bolland et al., 2020); **(i)** δ^{18}O of Gerzensee calcite (van Raden et al., 2013) and NGRIP (NGRIP members, 2004); **(j)** insolation curves for July (red) and December (blue). Lines indicate synchronous-time horizons across sites (shown at the bottom). Bottom, chronozones; AO, Aegelsee Oscillation; and GZ, Gerzensee Oscillation.

5.1.2 Bølling/Allerød (14.69–12.90 ka cal BP)

In the North Atlantic domain, the onset of the Bølling (start of DOE-1) shows a very sharp increase in δ^{18}O values in Greenland ice cores (Rasmussen et al., 2014). *Juniper* expanded rapidly on the Swiss Plateau, indicating an immediate response of terrestrial plants to the rapid warming that occurred within decades (Lotter et al., 1992). Amsoldingersee became only slightly more productive. Total aquatic production follows chironomid-inferred July temperatures with positive trends rather than the saw-tooth structure of annual temperatures, as shown by the NGRIP δ^{18}O or $\delta^{18}O_{CaCO3}$ records from Gerzensee (Lotter et al., 2012; Fig. 9i), suggesting that aquatic production mostly responded to warm-season temperatures. Whilst this is true for most algal groups, APB thrived during the short cold and dusty intervals of the Aegelsee and Gerzensee oscillations when winter ice cover was prolonged and hypolimnetic anoxia prevailed (Fig. 9). This supports the interpretation of both cold intervals being predominantly a phenomenon of the winter season cooling

that had little impact on summer temperatures (Lotter et al., 2012; Ammann et al., 2013). Apart from these cold intervals, we do not find any indication of lake stratification and hypolimnetic anoxia during the Bølling/Allerød warm phases. This finding is surprising considering warm summer temperatures and closed forest cover (arboreal pollen $> 80\,\%$, S4, Lotter et al., 1992), which typically lead to lake stratification and anoxia (Zander et al., 2021). Seemingly, summer thermal stratification and aquatic PP were not strong enough to initiate summer anoxia.

Significant blooms of silicifying algal groups are noted after the LST deposition (Fig. 8), suggesting an Si fertilisation effect of the tephra in the oligotrophic and possibly Si-limited lake. This effect lasted < 100 years and was also observed in the oligotrophic Moossee and Lobsigensee on the Swiss Plateau (Makri et al., 2020; Züllig, 1986).

5.1.3 Younger Dryas (12.90–11.7 ka cal BP)

The Younger Dryas (YD) was a cold phase in the North Atlantic region (Brauer et al., 2008) that was accompanied by a reduced Atlantic Meridional Overturning Circulation (AMOC; Böhm et al., 2015) and enhanced insolation-driven seasonality in this region (Fig. 9j). In Lobsigensee (Fig. 1b), Züllig (1986) observed extensive winter anoxia, which Züllig related to extended ice cover during very cold winters. Although summer temperatures decreased markedly during the YD (Heiri et al., 2015), total pigment concentrations remained high in Amsoldingersee, even after the fertilising effect of the LST disappeared, suggesting that warm summer temperature were no longer a controlling factor for algal growth.

The strong response of silicifiers to the LST suggests that the system was Si-limited at the end of the Allerød (before the LST). At the beginning of the YD, green algae (lutein, Fig. 8) decreased, whereas silicifiers (alloxanthin, diatoxanthin) remained high, suggesting that Si fertilisation related to persistently high dust fluxes (Ti, Fig. 9g) played a role. It is unlikely that enhanced P recycling under anoxic conditions stimulated aquatic PP during that time because redox-sensitive P, Fe, and Mn were sequestered rather than released (Fig. 5).

In Amsoldingersee, during the YD, we find multiple changes in productivity and anoxia, suggesting that the YD was not a homogenous cold phase but had an internal structure (Pigati and Springer, 2022; Weber et al., 2020). The YD started with ~ 185 years of low Tchl and high Bphe *a* (Fig. 9a and b), interpreted as a period with reduced epilimnetic production, short summers, and long-lasting winter stratification, similar to the findings of Brauer et al. (2008) in Meerfelder Maar. During the second part of the YD, productivity and anoxia covaried, and sequestration of redox-sensitive Fe, Mn, and P increased (transition from Cluster 3 to Cluster 4, Fig. 5). The end of the YD was associated with a drier climate, leading to lake-level lowering (Lotter and Boucherle, 1984). Dry conditions at the end of the YD were also found at other European sites (Weber et al., 2020; Brauer et al., 2008), consistent with the idea of gradually northward-shifting storm tracks throughout the Younger Dryas (Bakke et al., 2009, Fig. 9e).

5.1.4 The Late Glacial dust record

After 16.2 ka cal BP, the composition of clastic sediments in Lake Amsoldingen changed (PC2, Fig. 4). Ca, Sr, and TIC sharply dropped, whereas Ti, K, Si, and Zr remained at high levels, suggesting that there are two different sources of clastic sediments: one carbonate-dominated fraction (PC2 negative) related to erosion of calcareous glacial deposits in the lake catchment (low in siliciclastics) and another fraction of siliciclastic material (PC2 positive) likely related to allochthonous aeolian dust. The elevated and isolated topography of the Amsoldingersee catchment excludes fluvial transport as a potential source of siliciclastics (Fig. 1a).

The interpretation of the Ti, Si, and Zr records in Amsoldingersee as aeolian dust is supported by the similarity of Ti to NGRIP dust (NGRIP members, 2004, $R^2_{\mathrm{adj}} = 0.8$ by linear regression, Fig. 9g), showing relatively high values during H1 and the Younger Dryas (YD) and relatively lower values during the Bølling/Allerød and the early Holocene. Local dust maxima are observed in the NGRIP and Amsoldingen sediments, also synchronously during the cold episodes of the Aegelsee Oscillation (AO; 14.1 ka cal BP) and the Gerzensee Oscillation (GZ; 13.2 ka cal BP). While NGRIP dust is mainly sourced from Europe and central Asia (Újvári et al., 2015), a large part of the dust deposited across Europe was sourced from sparsely vegetated steppes of the English Channel and the North Sea (Rousseau et al., 2014). The similarity between the Amsoldingersee and the NGRIP dust records supports the view that the same large-scale atmospheric circulation patterns affected the Swiss Plateau and Greenland (Eicher, 1987; Lotter et al., 1992; Ammann et al., 2013).

Across Europe, aeolian deposits are well documented for the H1, the AO, and the Younger Dryas (Hoek et al., 2017). Estimated sedimentation rates for loess deposition range between 0.02 and $0.2\,\mathrm{mm\,yr^{-1}}$ during Heinrich events across European sites (Rousseau et al., 2021). Given the lithological composition of the catchment with a predominance of calcareous glacial deposits over silicate-bearing lithologies and the low sedimentation rates in Amsoldingersee (SAR of $0.1\,\mathrm{mm\,yr^{-1}}$; Fig. 2), dust fluxes on the above order of magnitude should be visible. Within Switzerland, the Etang de la Gruère peat bog record is, to date, the only site that describes dust fluxes in the Late Glacial. Similarly, Ti has been used as a dust proxy (Shotyk et al., 2001). While the Etang de Gruère record covers the Holocene (0–14.6 ka cal BP), the Amsoldingersee record is, to our knowledge, the first continuous record of aeolian dust covering the Late Glacial period (16–11 ka cal BP).

5.2 What drove the algal community composition?

Overall, algal community changes are synchronous with lithotype transitions and phases with high RoC (Fig. 8), which match the transitions of the chrono- and biostratigraphic zones, reflecting large-scale climatic variations in the North Atlantic domain (Ammann et al., 2013). Redundancy analysis indicates that aquatic primary production in Amsoldingersee (e.g., Tchl, total carotenoids) covaries with TOC and follows temperature and arboreal pollen predominantly but not exclusively (RDA, Fig. S9). Our data reveal that nutrients and lake mixing also played an essential role in shaping primary producer communities. Several lines of evidence suggest that P, N, and Si in the photic zone limited aquatic PP, although they have a changed relative importance over time.

Firstly, there is very little phosphorus sequestered throughout the entire record. In contrast to Soppensee (Tu et al., 2021), bioavailable P is barely present in Amsoldingersee (Fig. 5), despite well-mixed and oxic conditions during the more productive Bølling/Allerød, suggesting that P might have been particularly limited. Successions between algal groups provide a second line of evidence for the limitation of nutrients (P, possibly also N). While the climate warming at the beginning of the Bølling was very rapid and instantaneous (Bolland et al., 2020; Heiri et al., 2015; van Raden et al., 2013; Lotter et al., 2012), the response of the pigments (aquatic communities) was gradual, following a succession across ca. 500 years from astaxanthin (end of PZ 2c, Fig. 8) to chloroxanthin (PNSB), diatoxanthin (diatoms), echinenone (cyanobacteria), and lutein (green algae). This suggests that, at the onset of the Bølling, primary producer communities possibly did not predominantly respond to temperature but rather to nutrient availability. The timing of the algal succession is matched by successive increases in redox Mn, C/N, S, and eventually P_{org} (Fig. 8).

Secondly, nitrogen was likely limited during H1 and the onset of the Bølling. At the onset of H1, carotenoids associated with filamentous cyanobacteria (N fixing, Thiel, 2004) contribute considerably to the total carotenoids. Moreover, phycocyanin and Tchl covary, suggesting that a large share of Chlorophyll *a* (Tchl) was produced by cyanobacteria. As mentioned above, the algal response to the Bølling warming was relatively gradual, starting with astaxanthin and chloroxanthin (PNSB). Astaxanthin is a UV-protective carotenoid that *Haematococcus pluvialis* can use to store nutrients, which has been interpreted as N limitation and light stress (Orosa et al., 2001; Boussiba and Vonshak, 1991). Moreover, chloroxanthin is a pigment which is produced by purple nonsulfur bacteria of the *Rhodospirillum* or *Rhodobacter* genera, which are known nitrogen fixers (Albrecht et al., 1997; Keskin et al., 2011). Filamentous N-fixing cyanobacteria (canthaxanthin and echinenone) remained abundant during the Allerød and YD, suggesting that cyanobacteria still had a competitive advantage in N-limited conditions.

Lastly, at the beginning of the Bølling, a shift from silicifiers (diatoxanthin) to green algae (lutein) suggests Si limitation. This coincides with a decrease in dust (Ti) deposition (Fig. 9g). Further, after substantial Si fertilisation by the LST (13.05–12.90 ka cal BP; Fig. 8), we observe a response of silicifiers (Fig. 8), while green algae (lutein and Chl *a* and related pigments) and cyanobacteria remained invariant. Blooms of diatoxanthin (diatoms) and alloxanthin (cryptophytes) persisted during the YD, suggesting that Si fertilisation persisted throughout the YD. It is unusual to find signs of aerial silica fertilisation related to the tephra (Züllig, 1986) or dust in lake sediment records because these typically contain substantial siliciclastic fractions (Koffman et al., 2021).

5.3 Ice-induced anoxia in Late Glacial Amsoldingersee

Amsoldingersee documents four phases with hypolimnetic anoxia, all of which are related to cold periods: during H1, the Aegelsee Oscillation, the Gerzensee Oscillation, and the Younger Dryas. This is consistent with findings from Züllig (1986) in Lobsigensee (Fig. 1b), who documented anoxia during cold periods of the "Oldest Dryas" (H1) and the Younger Dryas and related these to prolonged winter ice cover. Although little is known about winter limnology (Jansen et al., 2021; Hampton et al., 2017), there is increasing evidence that extensive winter ice cover leads to anoxia in shallow lakes at high latitudes (Klanten et al., 2023). These conditions likely occurred in Switzerland during the cold phases of the Late Glacial. Many studies from the Arctic and Antarctica (Schütte et al., 2016; Reuss et al., 2013; Comeau et al., 2012; Rogozin et al., 2009; Karr et al., 2003) show that APB and PNSB are well adapted to light limitation under ice cover as they use bacteriochlorophyll *a*, which absorbs light at 550–600 nm, where transmittance through ice is maximal (Bolsenga et al., 1991). Pigments used by other organisms (e.g., Bchl *c*, *e*, *d* and Chl *a*, *b*) absorb light only at the edges of the light spectra transmitted through snow and ice (< 480 and > 630 nm; Zander et al., 2023; Stomp et al., 2007).

Our results and those of Züllig (1986) are in contrast with previous findings in Längsee (Schmidt et al., 2002) and Soppensee (Tu et al., 2021). Both lakes developed anoxia during the warm phases of the Late Glacial and not during the cold phases. The authors proposed a chemical feedback model in which summer warming leads to high aquatic PP, lake stratification, and anoxia, which prompt reductive dissolution of redox-sensitive metal oxides and recycling of nutrients, thus sustaining high aquatic PP and hypolimnetic anoxia (Gächter et al., 1988; Nürnberg, 1998). The different behaviours of these four lakes are surprising because they are very similar in terms of climatic and environmental background conditions. Our current understanding is too limited to provide a sound explanation for this discrepancy.

Amsoldingersee and Lobsigensee also developed anoxia at times of tundra vegetation (during H1) and reduced forest cover during the YD (Rey et al., 2020), whereas the lake

remained well mixed during the Allerød with closed pine forest. This stands in contrast to many small lakes across Europe that show anoxia during Holocene warm conditions. In such lakes, reduced wind mixing through closed forest covers (arboreal pollen > 80 %) prompted summer stratification with anoxia (Zander et al., 2021). In contrast, in Amsoldingersee, the winter ice cover was more important than the closed forest, prompting anoxia during Late Glacial conditions. This phenomenon is, however, not sufficiently well understood.

6 Conclusions

This study provides a contextual view of the complex interactions between climate variability (warming and cooling), aquatic primary production and primary producer communities, lake mixing regimes, anoxia, and nutrient cycling in a small glacial lake (Amsoldingersee) on the Swiss Plateau during Late Glacial times. This period is characterised by rapid and high-amplitude climatic changes during 18–11 ka cal BP, including Heinrich Stadial 1, the Bølling/Allerød, the Younger Dryas, and the onset of the Holocene. We hypothesise that the responses of lakes in early deglacial Switzerland can be used as analogies for modern lakes in the Arctic under rapid warming.

In Amsoldingersee, changes in aquatic primary production and algal (pigment) communities are synchronous with changes in lithotypes, biostratigraphy in the catchment, and large-scale climatic changes in the North Atlantic domain. Aquatic PP and algal communities were driven mainly by summer temperature but were strongly modulated by nutrient limitations (P, N, Si) throughout Late Glacial times. Anoxic phases changed the algal communities, but these shifts were fully reversible once anoxia vanished. Noteworthy are differences in the pigment preservation and grazing pressure before and after anoxia. The first significant increase in aquatic PP is observed during H1, around 16.1 ka cal BP, i.e. much earlier than the Bølling warming at 14.6 ka cal BP.

Our record reveals four anoxic phases during Late Glacial times; all of them occurred under cold periods with prolonged ice cover during H1 (16 ka cal BP), the Aegelsee and Gerzensee oscillations, and the YD. During the warm Bølling/Allerød, the lake remained well mixed. These results contrast with findings from other lakes (Switzerland, Austria), where anoxia occurred during warm periods of the Late Glacial. This discrepancy is surprising since these lakes are in similar climatic conditions and have similar morphometry, suggesting that very subtle differences may lead to diverse responses of similar lakes to the same climatic forcing. The reasons for this discrepancy are currently poorly understood, but they possibly reflect the very complex responses of small lakes to rapid warming as presently observed in the Arctic.

The sediments of Amsoldingersee provide a unique continuous record of dust deposition (Ti, Zr, and Si) covering the complete Late Glacial period (18–11 ka cal BP). This record very closely matches the NGRIP dust record, confirming earlier findings that both regions (Swiss Plateau and Greenland) are linked through large-scale climate phenomena. Similar to the strong Si-fertilising effect of the Laacher See tephra in Amsoldingersee, atmospheric dust also seems to have modulated the primary production of silicifying algae during the Bølling/Allerød and the YD.

Code and data availability. Pre-processed data are available at Pangaea (https://doi.org/10.1594/PANGAEA.975327, Schouten et al., 2025a, https://doi.org/10.1594/PANGAEA.975263, Schouten et al., 2025b, https://doi.org/10.1594/PANGAEA.975261, Schouten et al., 2025c), and code is available at GitHub (Schouten, 2024a, b, 2025a, b).

Supplement. The supplement related to this article is available online at https://doi.org/10.5194/bg-22-3821-2025-supplement.

Author contributions. SJS – conceptualisation, formal analysis and investigation, visualisation and coding, writing of original draft. PZ – conceptualisation, XRF data curation, formal analysis and investigation, co-supervision. NRMMS – conceptualisation, formal analysis and investigation. AL – HPLC, pigment interpretation. PBK – macrofossil identification. JFNvL – pollen analysis. HV – co-supervision. MG – conceptualisation, supervision, interpretation, and contribution to writing the original draft. SJS, PZ, MG, NRMMS, and HV commented; SJS, PZ, HV, and MG edited; and all co-authors approved the paper.

Competing interests. The contact author has declared that none of the authors has any competing interests.

Disclaimer. Publisher's note: Copernicus Publications remains neutral with regard to jurisdictional claims made in the text, published maps, institutional affiliations, or any other geographical representation in this paper. While Copernicus Publications makes every effort to include appropriate place names, the final responsibility lies with the authors.

Acknowledgements. We thank Willy Tanner for leading the coring campaign and the staff at the Institutes of Geography and Geology for support in the lab. We thank Wolfgang Hegner for granting us access to the lake and Thomas Ernst for supporting us on the site. LANAT provided the research permission. We further thank Rik Tjallingii for his help in processing XRF data and valuable comments on the paper. Lastly, we thank the two reviewers for their constructive and supportive feedback.

Financial support. This research has been supported by the Schweizerischer Nationalfonds zur Förderung der Wissenschaftlichen Forschung (grant no. 200020_204220).

Review statement. This paper was edited by Petr Kuneš and reviewed by Pierre Francus and one anonymous referee.

References

Aitchison, J.: The statistical analysis of compositional data, J. Roy. Stat. Soc. B Met., 44, 139–160, 1982.

Albrecht, M., Ruther, A., and Sandmann, G.: Purification and biochemical characterization of a hydroxyneurosporene desaturase involved in the biosynthetic pathway of the carotenoid spheroidene in Rhodobacter sphaeroides, J. Bacteriol., 179, 7462–7467, https://doi.org/10.1128/jb.179.23.7462-7467, 1997.

Ammann, B., van Leeuwen, J. F., van der Knaap, W. O., Lischke, H., Heiri, O., and Tinner, W.: Vegetation responses to rapid warming and to minor climatic fluctuations during the Late-Glacial Interstadial (GI-1) at Gerzensee (Switzerland), Palaeogeogr. Palaeocl., 391, 40–59, https://doi.org/10.1016/j.palaeo.2012.07.010, 2013.

Bakke, J., Lie, Ø., Heegaard, E., Dokken, T., Haug, G. H., Birks, H. H., Dulski, P., and Nilsen, T.: Rapid oceanic and atmospheric changes during the Younger Dryas cold period, Nat. Geosci., 2, 202–205, https://doi.org/10.1038/ngeo439, 2009.

Bertrand, S., Tjallingii, R., Kylander, M. E., Wilhelm, B., Roberts, S. J., Arnaud, F., Brown, E., and Bindler, R.: Inorganic geochemistry of lake sediments: A review of analytical techniques and guidelines for data interpretation, Earth-Sci. Rev., 249, 104639, https://doi.org/10.1016/j.earscirev.2023.104639, 2023.

Bianchi, T. S. and Canuel, E. A.: Photosynthetic Pigments: Chlorophylls, Carotenoids, and Phycobilins, in: Chemical Biomarkers in Aquatic Ecosystems, edited by: Bianchi, T. S. and Canuel, E. A., Princeton University Press, 221–247, https://doi.org/10.1515/9781400839100, 2011.

Blaauw, M. and Christen, J. A.: Flexible paleoclimate age-depth models using an autoregressive gamma process, Bayesian Anal., 6, 457–474, https://doi.org/10.1214/11-BA618, 2011.

Böhm, E., Lippold, J., Gutjahr, M., Frank, M., Blaser, P., Antz, B., Fohlmeister, J., Frank, N., Andersen, M. B., and Deininger, M.: Strong and deep Atlantic meridional overturning circulation during the last glacial cycle, Nature, 517, 73–76, https://doi.org/10.1038/ngeo439, 2015.

Bolland, A., Rey, F., Gobet, E., Tinner, W., and Heiri, O.: Summer temperature development 18,000–14,000 cal. BP recorded by a new chironomid record from Burgäschisee, Swiss Plateau, Quaternary Sci. Rev., 243, 106484, https://doi.org/10.1016/j.quascirev.2020.106484, 2020.

Bolsenga, S. J., Herdendorf, C. E., and Norton, D. C.: Spectral transmittance of lake ice from 400–850 nm, Hydrobiologia, 218, 15–25, https://doi.org/10.1007/BF00006414, 1991.

Bos, I. J., Busschers, F. S., and Hoek, W. Z.: Organic-facies determination: a key for understanding facies distribution in the basal peat layer of the Holocene Rhine-Meuse delta, The Netherlands, Sedimentology, 59, 676–703, https://doi.org/10.1111/j.1365-3091.2011.01271.x, 2012.

Boussiba, S. and Vonshak, A.: Astaxanthin accumulation in the green alga *Haematococcus pluvialis*, Plant Cell Physiol., 32, 1077–1082, https://doi.org/10.1093/oxfordjournals.pcp.a078171, 1991.

Brauer, A., Haug, G. H., Dulski, P., Sigman, D. M., and Negendank, J. F.: An abrupt wind shift in western Europe at the onset of the Younger Dryas cold period, Nat. Geosci., 1, 520–523, https://doi.org/10.1038/ngeo263, 2008.

Brodie, C. R., Casford, J. S., Lloyd, J. M., Leng, M. J., Heaton, T. H., Kendrick, C. P., and Yongqiang, Z.: Evidence for bias in C/N, δ^{13}C and δ^{15}N values of bulk organic matter, and on environmental interpretation, from a lake sedimentary sequence by pre-analysis acid treatment methods, Quaternary Sci. Rev., 30, 3076–3087, https://doi.org/10.1016/j.quascirev.2011.07.003, 2011.

Buchaca, T. and Catalan, J.: On the contribution of phytoplankton and benthic biofilms to the sediment record of marker pigments in high mountain lakes, J. Paleolimnol., 40, 369–383, https://doi.org/10.1007/s10933-007-9167-1, 2008.

Bush, T., Diao, M., Allen, R. J., Sinnige, R., Muyzer, G., and Huisman, J.: Oxic-anoxic regime shifts mediated by feedbacks between biogeochemical processes and microbial community dynamics, Nat. Commun., 8, 789, https://doi.org/10.1038/s41467-017-00912-x, 2017.

Butz, C., Grosjean, M., Fischer, D., Wunderle, S., Tylmann, W., and Rein, B.: Hyperspectral imaging spectroscopy: a promising method for the biogeochemical analysis of lake sediments, J. Appl. Remote Sens., 9, 096031, https://doi.org/10.1117/1.JRS.9.096031, 2015.

Carey, C. C., Hanson, P. C., Thomas, R. Q., Gerling, A. B., Hounshell, A. G., Lewis, A. S., Lofton, M. E., McClure, R. P., Wander, H. L., Woelmer, W. M., Niederlehner, B. R., and Schreiber M. E.: Anoxia decreases the magnitude of the carbon, nitrogen, and phosphorus sink in freshwaters, Glob. Change Biol., 28, 4861–4881, https://doi.org/10.1002/essoar.10508415.3, 2022.

Comeau, A. M., Harding, T., Galand, P. E., Vincent, W. F., and Lovejoy, C.: Vertical distribution of microbial communities in a perennially stratified Arctic lake with saline, anoxic bottom waters, Sci. Rep., 2, 604, https://doi.org/10.1038/srep00604, 2012.

Eicher, U.: Die spätglazialen sowie die frühpostglazialen Klimaverhältnisse im Bereiche der Alpen : Sauerstoffisotopenkurven kalkhaltiger Sedimente, Geogr. Helv., 42, 99–104, https://doi.org/10.5194/gh-42-99-1987, 1987.

Eicher, U.: Stable oxygen and carbon isotope analyses on lacustrine carbonate sediments, in: Problems of Stable Isotopes in Tree-rings, Lake Sediments and Peat-bogs as Climatic Evidence for the Holocene, Paläoklimaforschung, G. Fischer, Stuttgart, 29–38, https://doi.org/10.1130/G46593.1, 1995.

Fabbri, S. C., Buechi, M. W., Horstmeyer, H., Hilbe, M., Hübscher, C., Schmelzbach, C., Weiss, B., and Anselmetti, F. S.: A subaquatic moraine complex in overdeepened Lake Thun (Switzerland) unravelling the deglaciation history of the Aare Glacier, Quaternary Sci. Rev., 187, 62–79, https://doi.org/10.1016/j.quascirev.2018.03.010, 2018.

Foley, B., Jones, I. D., Maberly, S. C., and Rippey, B.: Long-term changes in oxygen depletion in a small temperate lake: effects of climate change and eutrophication, Freshwater Biol., 57, 278–289, https://doi.org/10.1111/j.1365-2427.2011.02662.x, 2012.

Friedrich, J., Janssen, F., Aleynik, D., Bange, H. W., Boltacheva, N., Çagatay, M. N., Dale, A. W., Etiope, G., Erdem, Z., Geraga, M., Gilli, A., Gomoiu, M. T., Hall, P. O. J., Hansson, D., He, Y., Holtappels, M., Kirf, M. K., Kononets, M., Konovalov, S., Lichtschlag, A., Livingstone, D. M., Marinaro, G., Mazlumyan, S., Naeher, S., North, R. P., Papatheodorou, G.,

Pfannkuche, O., Prien, R., Rehder, G., Schubert, C. J., Soltwedel, T., Sommer, S., Stahl, H., Stanev, E. V., Teaca, A., Tengberg, A., Waldmann, C., Wehrli, B., and Wenzhöfer, F.: Investigating hypoxia in aquatic environments: diverse approaches to addressing a complex phenomenon, Biogeosciences, 11, 1215–1259, https://doi.org/10.5194/bg-11-1215-2014, 2014.

Gächter, R., Meyer, J. S., and Mares, A.: Contribution of bacteria to release and fixation of phosphorus in lake sediments, Limnol. Oceanogr., 33, 1542–1558, https://doi.org/10.4319/lo.1988.33.6_part_2.1542, 1988.

Gilarranz, L. J., Narwani, A., Odermatt, D., Siber, R., and Dakos, V.: Regime shifts, trends, and variability of lake productivity at a global scale, P. Natl. Acad. Sci. USA, 119, e2116413119, https://doi.org/10.1073/pnas.2116413119, 2022.

Grimm, E. C.: CONISS: a FORTRAN 77 program for stratigraphically constrained cluster analysis by the method of incremental sum of squares, Comput. Geosci., 13, 13–35, https://doi.org/10.1016/0098-3004(87)90022-7, 1987.

Guthruf, K, Maurer, V., Ryser, R., Zeh, M., and Zweifel, N.: Amsoldingersee, in Zustand der Kleinseen, Awa Fakten, Bau-, Verkehrs- und Energiedirektion des Kantons Bern, 35–42, 2015.

Hampton, S. E., Galloway, A. W. E., Powers, S. M., Ozersky, T., Woo, K. H., Batt, R. D., Labou, S. G., O'Reilly, C. M., Sharma, S., Lottig, N. R., Stanley, E. H., North, R. L., Stockwell, J. D., Adrian, R., Weyhenmeyer, G. A., Arvola, L., Baulch, H. M., Bertani, I., Bowman Jr., L. L., Carey, C. C., Catalan, J., Colom-Montero, W., Domine, L. M., Felip, M., Granados, I., Gries, C., Grossart, H.-P., Haberman, J., Haldna, M., Hayden, B., Higgins, S. N., Jolley, J. C., Kahilainen, K. K., Kaup, E., Kehoe, M. J., MacIntyre, S., Mackay, A. W., Mariash, H. L., McKay, R. M., Nixdorf, B., Nõges, P., Nõges, T., Palmer, M., Pierson, D. C., Post, D. M., Pruett, M. J., Rautio, M., Read, J. S., Roberts, S. L., Rücker, J., Sadro, S., Silow, E. A., Smith, D. E., Sterner, R. W., Swann, G. E. A., Timofeyev, M. A., Toro, M., Twiss, M. R., Vogt, R. J., Watson, S. B., Whiteford, E. J., and Xenopoulos, M. A.: Ecology under lake ice, Ecol. Lett., 20, 98–111, https://doi.org/10.1111/ele.12699, 2017.

Heiri, O., Ilyashuk, B., Millet, L., Samartin, S., and Lotter, A. F.: Stacking of discontinuous regional palaeoclimate records: Chironomid-based summer temperatures from the Alpine region, Holocene, 25, 137–149, https://doi.org/10.1177/0959683614556382, 2015.

Hoek, W. Z., Lammertsma, E. I., Bohncke, S. J., Bos, J. A., Bunnik, F., Kasse, C., Schokker, J., and Westerhoff, W.: Lateglacial and early Holocene vegetation development and fluvial system changes in the northern Meuse valley, the Netherlands: a review of palynological data, Neth. J. Geosci., 96, 93–114, https://doi.org/10.1017/njg.2017.4, 2017.

Hupfer, M. and Lewandowski, J.: Oxygen controls the phosphorus release from lake sediments–a long-lasting paradigm in limnology, Int. Rev. Hydrobiol., 93, 415–432, https://doi.org/10.1002/iroh.200711054, 2008.

Ivy-Ochs, S., Kerschner, H., Kubik, P. W., and Schlüchter, C.: Glacier response in the European Alps to Heinrich Event 1 cooling: the Gschnitz stadial, J. Quaternary Sci., 21, 115–130, https://doi.org/10.1002/jqs.955, 2006.

Jane, S. F., Hansen, G. J. A., Kraemer, B. M., Leavitt, P. R., Mincer, J. L., North, R. L., Pilla, R. M., Stetler, J. T., Williamson, C. E., Woolway, R. I., Arvola, L., Chandra, S., DeGasperi, C. L., Diemer, L., Dunalska, J., Erina, O., Flaim, G., Grossart, H.-P., Hambright, K. D., Hein, C., Hejzlar, J., Janus, L. L., Jenny, J.-P., Jones, J. R., Knoll, L. B., Leoni, B., Mackay, E., Matsuzaki, S.-I. S., McBride, C., Müller-Navarra, D. C., Paterson, A. M., Pierson, D., Rogora, M., Rusak, J. A., Sadro, S., Saulnier-Talbot, E., Schmid, M., Sommaruga, R., Thiery, W., Verburg, P., Weathers, K. C., Weyhenmeyer, G. A., Yokota, K., and Rose, K. C.: Widespread deoxygenation of temperate lakes, Nature, 594, 66–70, https://doi.org/10.1038/s41586-021-03550-y, 2021.

Jansen, J., MacIntyre, S., Barrett, D. C., Chin, Y.-P., Cortés, A., Forrest, A. L., Hrycik, A. R., Martin, R., McMeans, B. C., Rautio, M., and Schwefel, R.: Winter limnology: how do hydrodynamics and biogeochemistry shape ecosystems under ice?, J. Geophys. Res.-Biogeo., 126, e2020JG006237, https://doi.org/10.5194/egusphere-egu21-1693, 2021.

Jansen, J., Simpson, G. L., Weyhenmeyer, G. A., Härkönen, L. H., Paterson, A. M., del Giorgio, P. A., and Prairie, Y. T.: Climate-driven deoxygenation of northern lakes, Nat. Clim. Change, 14, 832–838, https://doi.org/10.1038/s41558-024-02058-3, 2024.

Jeffrey, S. T. and Humphrey, G. F.: New spectrophotometric equations for determining chlorophylls a, b, $c1$ and $c2$ in higher plants, algae and natural phytoplankton, Biochem. Physiol. Pfl., 167, 191–194, https://doi.org/10.1016/s0015-3796(17)30778-3, 1975.

Jenny, J.-P., Francus, P., Normandeau, A., Lapointe, F., Perga, M.-E., Ojala, A., Schimmelmann, A., Zolitschka, B.: Global spread of hypoxia in freshwater ecosystems during the last three centuries is caused by rising local human pressure, Glob. Change Biol., 22, 1481–1489, https://doi.org/10.1111/gcb.13193, 2016.

Jeppesen, E., Moss, B., Bennion, H., Carvalho, L., DeMeester, L., Feuchtmayr, H., Friberg, N., Gessner, M. O., Hefting, M., Lauridsen, T. L., Liboriussen, L., Malmquist, H. J., May, L., Meerhoff, M., Olafsson, J. S., Soons, M. B., and Verhoeven, J. T. A.: Interaction of Climate Change and Eutrophication, in: Climate Change Impacts on Freshwater Ecosystems, edited by: Kernan, M., Battarbee, R. W., and Moss, B., Wiley, 119–151, https://doi.org/10.1002/9781444327397.ch6, 2010.

Karr, E. A., Sattley, W. M., Jung, D. O., Madigan, M. T., and Achenbach, L. A.: Remarkable diversity of phototrophic purple bacteria in a permanently frozen Antarctic lake, Appl. Environ. Microb., 69, 4910–4914, https://doi.org/10.1128/aem.69.8.4910-4914.2003, 2003.

Keskin, T., Abo-Hashesh, M., and Hallenbeck, P. C.: Photofermentative hydrogen production from wastes, Bioresource Technol., 102, 8557–8568, https://doi.org/10.1016/j.biortech.2011.04.004, 2011.

Klanten, Y., Couture, R.-M., Christoffersen, K. S., Vincent, W. F., and Antoniades, D.: Oxygen depletion in Arctic lakes: circumpolar trends, biogeochemical processes, and implications of climate change, Global Biogeochem. Cy., 37, e2022GB007616, https://doi.org/10.1029/2022gb007616, 2023.

Koffman, B. G., Yoder, M. F., Methven, T., Hanschka, L., Sears, H. B., Saylor, P. L., and Wallace, K. L.: Glacial dust surpasses both volcanic ash and desert dust in its iron fertilization potential, Global Biogeochem. Cy., 35, e2020GB006821, https://doi.org/10.1029/2020gb006821, 2021.

Kramer, S. J. and Siegel, D. A.: How can phytoplankton pigments be best used to characterize surface ocean phytoplankton groups for ocean color remote sensing algorithms?, J. Geophys. Res.-

Oceans, 124, 7557–7574, https://doi.org/10.1029/2019jc015604, 2019.

Lami, A., Guilizzoni, P., and Marchetto, A.: High resolution analysis of fossil pigments, carbon, nitrogen and sulphur in the sediment of eight European Alpine lakes: The MOLAR project, J. Limnol., 59, 15–28, https://doi.org/10.4081/jlimnol.2000.s1.15, 2000.

Lami, A., Musazzi, S., Marchetto, A., Buchaca, T., Kernan, M., Jeppesen, E., and Guilizzoni, P.: Sedimentary pigments in 308 alpine lakes and their relation to environmental gradients, Adv. Limnol., 62, 247–268, https://doi.org/10.1127/advlim/62/2009/247, 2009.

Leavitt, P. R. and Hodgson, D. A.: Sedimentary pigments, in: Tracking environmental change using lake sediments: Terrestrial, algal, and siliceous indicators, edited by: Smol, J. P., Birks, H. J. B., Last, W. M., Bradley, R. S., and Alverson, K., Springer, Dordrecht, the Netherlands, 295–325, https://doi.org/10.1007/0-306-47668-1_15, 2001.

Legendre, P.: Numerical ecology, Elsevier, https://doi.org/10.1016/b978-0-12-409548-9.10595-0, 2012.

Lévesque, B., Gervais, M. C., Chevalier, P., Gauvin, D., Anassour-Laouan-Sidi, E., Gingras, S., Fortin, N., Brisson, B., Greer, C., and Bird, D.: Prospective study of acute health effects in relation to exposure to cyanobacteria, Sci. Total Environ., 466, 397–403, https://doi.org/10.1016/j.scitotenv.2013.07.045, 2014.

Lotter, A. and Boucherle, M. M.: A late-glacial and post-glacial history of Amsoldingersee and vicinity, Switzerland, Schweiz. Z. Hydrol., 46, 192–209, https://doi.org/10.1007/bf02538061, 1984.

Lotter, A. F., Eicher, U., Siegenthaler, U., and Birks, H. J.: Late-glacial climatic oscillations as recorded in Swiss lake sediments, J. Quaternary Sci., 7, 187–204, https://doi.org/10.1002/jqs.3390070302, 1992.

Lotter, A. F., Birks, H. J., Eicher, U., Hofmann, W., Schwander, J., and Wick, L.: Younger Dryas and Allerød summer temperatures at Gerzensee (Switzerland) inferred from fossil pollen and cladoceran assemblages, Palaeogeogr. Palaeocl., 159, 349–361,10.1016/s0031-0182(00)00093-6, 2000.

Lotter, A. F., Heiri, O., Brooks, S., van Leeuwen, J. F., Eicher, U., and Ammann, B.: Rapid summer temperature changes during Termination 1a: high-resolution multi-proxy climate reconstructions from Gerzensee (Switzerland), Quaternary Sci. Rev., 36, 103–113, https://doi.org/10.1016/j.quascirev.2010.06.022, 2012.

Luetscher, M., Boch, R., Sodemann, H., Spötl, C., Cheng, H., Edwards, R. L., Frisia, S., Hof, F., and Müller, W.: North Atlantic storm track changes during the Last Glacial Maximum recorded by Alpine speleothems, Nat. Commun., 6, 6344, https://doi.org/10.1038/ncomms7344, 2015.

Lukkari, K., Hartikainen, H., and Leivuori, M.: Fractionation of sediment phosphorus revisited. I: Fractionation steps and their biogeochemical basis, Limnol. Oceanogr.-Meth., 5, 433–444, https://doi.org/10.4319/lom.2007.5.433, 2007.

Makri, S., Rey, F., Gobet, E., Gilli, A., Tinner, W., and Grosjean, M.: Early human impact in a 15,000-year high-resolution hyperspectral imaging record of paleoproduction and anoxia from a varved lake in Switzerland, Quaternary Sci. Rev., 239, 106335, https://doi.org/10.1016/j.quascirev.2020.106335, 2020.

Meerhoff, M., Audet, J., Davidson, T. A., De Meester, L., Hilt, S., Kosten, S., Liu, Z., Mazzeo, N., Paerl, H., Scheffer, M., and Jeppesen E.: Feedback between climate change and eutrophication: revisiting the allied attack concept and how to strike back, Inland Waters, 12, 187–204, https://doi.org/10.1080/20442041.2022.2029317, 2022.

Meyers, P. A.: Organic geochemical proxies of paleoceanographic, paleolimnologic, and paleoclimatic processes, Org. Geochem., 27, 213–250, https://doi.org/10.1016/s0146-6380(97)00049-1, 1997.

Moore, P. D., Webb, J. A., and Collison, M. E. (Eds.): Pollen analysis, Blackwell Scientific Publications, Oxford, vii+266 pp., ISBN 9780632021765, 1991.

Mottl, O., Grytnes, J.-A., Seddon, A. W., Steinbauer, M. J., Bhatta, K. P., Felde, V. A., Flantua, S. G. A., and Birks, H. J. B.: Rate-of-change analysis in paleoecology revisited: A new approach, Rev. Palaeobot. Palyno., 293, 104483, https://doi.org/10.1016/j.revpalbo.2021.104483, 2021.

Myrbo, A., Morrison, A., and McEwan, R.: Tool for microscopic identification (TMI), LacCore, http://tmi.laccore.umn.edu (last access: 31 July 2025), 2011.

North Greenland Ice Core Project members: High-resolution record of Northern Hemisphere climate extending into the last interglacial period, Nature, 431, 147–151, https://doi.org/10.1038/nature02805, 2004.

Nürnberg, G. K.: Prediction of annual and seasonal phosphorus concentrations in stratified and polymictic lakes, Limnol. Oceanogr., 43, 1544–1552, https://doi.org/10.4319/lo.1998.43.7.1544, 1998.

Orosa, M., Valero, J. F., Herrero, C., and Abalde, J.: Comparison of the accumulation of astaxanthin in *Haematococcus pluvialis* and other green microalgae under N-starvation and high light conditions, Biotechnology Letters, 23, 1079–1085, https://doi.org/10.1023/A:1010510508384, 2001.

Pigati, J. S. and Springer, K. B.: Hydroclimate response of spring ecosystems to a two-stage Younger Dryas event in western North America, Sci. Rep., 12, 7323, https://doi.org/10.1038/s41598-022-11377-4, 2022.

Podani, J. and Miklós, I.: Resemblance coefficients and the horseshoe effect in principal coordinates analysis, Ecology, 83, 3331–3343, 2002.

Rasmussen, S. O., Bigler, M., Blockley, S. P., Blunier, T., Buchardt, S. L., Clausen, H. B., Cvijanovic, I., Dahl-Jensen, D., Johnsen, S. J., Fischer, H., Gkinis, V., Guillevic, M., Hoek, W. Z., Lowe, J. J., Pedro, J. B., Popp, T., Seierstad, I. K., Steffensen, J. P., Svensson, A. M., Vallelonga, P., Vinther, B. M., Walker, M. J. C., Wheatley, J. J., and Winstrup, M.: A stratigraphic framework for abrupt climatic changes during the Last Glacial period based on three synchronized Greenland ice-core records: refining and extending the INTIMATE event stratigraphy, Quaternary Sci. Rev., 106, 14–28, https://doi.org/10.1016/j.quascirev.2014.09.007, 2014.

Reimer, P. J., Austin, W. E. N., Bard, E., Bayliss, A., Blackwell, P. G., Ramsey, C. B., Butzin, M., Cheng, H., Edwards, R. L., Friedrich, M., Grootes, P. M., Guilderson, T. P., Hajdas, I., Heaton, T. J., Hogg, A. G., Hughen, K. A., Kromer, B., Manning, S. W., Muscheler, R., Palmer, J. G., Pearson, C., Plicht, J. van der, Reimer, R. W., Richards, D. A., Scott, E. M., Southon, J. R., Turney, C. S. M., Wacker, L., Adolphi, F., Büntgen, U., Capano, M., Fahrni, S. M., Fogtmann-Schulz, A., Friedrich, R., Köhler, P., Kudsk, S., Miyake, F., Olsen, J., Reinig, F., Sakamoto, M., Sookdeo, A., and Talamo, S.: The IntCal20 Northern Hemi-

sphere Radiocarbon Age Calibration Curve (0–55 cal kBP), Radiocarbon, 62, 725–757, https://doi.org/10.1017/RDC.2020.41, 2020.

Reinig, F., Wacker, L., Jöris, O., Oppenheimer, C., Guidobaldi, G., Nievergelt, D., Adolphi, F., Cherubini, P., Engels, S., Esper, J., Land, A., Lane, C., Pfanz, H., Remmele, S., Sigl, M., Sookdeo, A., and Büntgen, U.: Precise date for the Laacher See eruption synchronizes the Younger Dryas, Nature, 595, 66–69, https://doi.org/10.1038/s41586-021-03608-x, 2021.

Reuss, N. S., Anderson, N. J., Fritz, S. C., and Simpson, G. L.: Responses of microbial phototrophs to late-Holocene environmental forcing of lakes in south-west Greenland, Freshwater Biol., 58, 690–704, https://doi.org/10.1111/fwb.12073, 2013.

Rey, F., Gobet, E., Schwörer, C., Hafner, A., Szidat, S., and Tinner, W.: Climate impacts on vegetation and fire dynamics since the last deglaciation at Moossee (Switzerland), Clim. Past, 16, 1347–1367, https://doi.org/10.5194/cp-16-1347-2020, 2020.

Rey, F., Gobet, E., van Leeuwen, J. F., Gilli, A., van Raden, U. J., Hafner, A., Wey, O., Rhiner, J., Schmocker, D., Zünd, J., and Tinner, W.: Vegetational and agricultural dynamics at Burgäschisee (Swiss Plateau) recorded for 18,700 years by multi-proxy evidence from partly varved sediments, Veg. Hist. Archaeobot., 26, 571–586, https://doi.org/10.1007/s00334-017-0635-x, 2017.

Richardson, K., Steffen, W., Lucht, W., Bendtsen, J., Cornell, S. E., Donges, J. F., Drüke, M., Fetzer, I., Bala, G., Bloh, W. von, Feulner, G., Fiedler, S., Gerten, D., Gleeson, T., Hofmann, M., Huiskamp, W., Kummu, M., Mohan, C., Nogués-Bravo, D., Petri, S., Porkka, M., Rahmstorf, S., Schaphoff, S., Thonicke, K., Tobian, A., Virkki, V., Wang-Erlandsson, L., Weber, L., and Rockström, J.: Earth beyond six of nine planetary boundaries, Sci. Adv., 9, eadh2458, https://doi.org/10.1126/sciadv.adh2458, 2023.

Rogozin, D. Y., Zykov, V. V., Chernetsky, M. Y., Degermendzhy, A. G., and Gulati, R. D.: Effect of winter conditions on distributions of anoxic phototrophic bacteria in two meromictic lakes in Siberia, Russia, Aquat. Ecol., 43, 661–672, https://doi.org/10.1007/s10452-009-9270-7, 2009.

Romero-Viana, L., Keely, B. J., Camacho, A., Vicente, E., and Miracle, M. R.: Primary production in Lake La Cruz (Spain) over the last four centuries: reconstruction based on sedimentary signal of photosynthetic pigments, J. Paleolimnol., 43, 771–786, https://doi.org/10.1007/s10933-009-9367-y, 2010.

Rousseau, D.-D., Chauvel, C., Sima, A., Hatté, C., Lagroix, F., Antoine, P., Balkanski, Y., Fuchs, M., Mellet, C., Kageyama, M., Ramstein, G., Lang, A.: European glacial dust deposits: Geochemical constraints on atmospheric dust cycle modeling, Geophys. Res. Lett., 41, 7666–7674, https://doi.org/10.1002/2014gl061382, 2014.

Rousseau, D.-D., Antoine, P., and Sun, Y.: How dusty was the last glacial maximum over Europe?, Quaternary Sci. Rev., 254, 106775, https://doi.org/10.1016/j.quascirev.2020.106775, 2021.

Salk, K. R., Venkiteswaran, J. J., Couture, R.-M., Higgins, S. N., Paterson, M. J., and Schiff, S. L.: Warming combined with experimental eutrophication intensifies lake phytoplankton blooms, Limnol. Oceanogr., 67, 147–158, https://doi.org/10.1002/lno.11982, 2022.

Schaller, T. and Wehrli, B.: Geochemical-focusing of manganese in lake sediments—an indicator of deep-water oxygen conditions, Aquat. Geochem., 2, 359–378, https://doi.org/10.1007/bf00115977, 1996.

Schlüter, L., Lauridsen, T. L., Krogh, G., and Jørgensen, T.: Identification and quantification of phytoplankton groups in lakes using new pigment ratios – a comparison between pigment analysis by HPLC and microscopy, Freshwater Biol., 51, 1474–1485, https://doi.org/10.1111/j.1365-2427.2006.01582.x, 2006.

Schmidt, R., Psenner, R., Müller, J., Indinger, P., and Kamenik, C.: Impact of late glacial climate variations on stratification and trophic state of the meromictic lake Längsee (Austria): validation of a conceptual model by multi proxy studies, J. Limnol., 61, 49–60,10.4081/jlimnol.2002.49, 2002.

Scholtysik, G., Goldhammer, T., Arz, H. W., Moros, M., Littke, R., and Hupfer, M.: Geochemical focusing and burial of sedimentary iron, manganese, and phosphorus during lake eutrophication, Limnol. Oceanogr., 67, 768–783, https://doi.org/10.1002/lno.12019, 2022.

Schouten, S. J.: multiproxyplotter, GitHub repository [code], https://github.com/SJSchouten/multiproxyplotter, 2024a.

Schouten, S. J.: Pigment_Heatmaps, GitHub repository [code], https://github.com/SJSchouten/Pigment_Heatmaps, 2024b.

Schouten, S. J.: RDA, GitHub repository [code], https://github.com/SJSchouten/RDA, 2025a.

Schouten, S. J.: RoC, GitHub repository [code], https://github.com/SJSchouten/RoC, 2025b.

Schouten, S. J., Zahajská, P., Schmidhauser, N. R. M. M., Lami, A., van Leeuwen, J. F. N., Boltshauser-Kaltenrieder, P., Vogel, H., and Grosjean, M.: Pigments, sequential extraction, and CNS measurements of Amsoldingersee sediment core, Switzerland, PANGAEA [data set], https://doi.org/10.1594/PANGAEA.975327, 2025a.

Schouten, S. J., Zahajská, P., Schmidhauser, N. R. M. M., Lami, A., van Leeuwen, J. F. N., Boltshauser-Kaltenrieder, P., Vogel, H., and Grosjean, M.: XRF measurements of Amsoldingersee sediment core, Switzerland, PANGAEA [data set], https://doi.org/10.1594/PANGAEA.975263, 2025b.

Schouten, S. J., Zahajská, P., Schmidhauser, N. R. M. M., Lami, A., van Leeuwen, J. F. N., Boltshauser-Kaltenrieder, P., Vogel, H., and Grosjean, M.: Hyperspectral measurements of Amsoldingersee sediment core, Switzerland, PANGAEA [data set], https://doi.org/10.1594/PANGAEA.975261, 2025c.

Schütte, U. M., Cadieux, S. B., Hemmerich, C., Pratt, L. M., and White, J. R.: Unanticipated geochemical and microbial community structure under seasonal ice cover in a dilute, dimictic Arctic lake, Front. Microbiol., 7, 1035, https://doi.org/10.3389/fmicb.2016.01035, 2016.

Shotyk, W., Weiss, D., Kramers, J. D., Frei, R., Cheburkin, A. K., Gloor, M., and Reese, S.: Geochemistry of the peat bog at Etang de la Gruère, Jura Mountains, Switzerland, and its record of atmospheric Pb and lithogenic trace metals (Sc, Ti, Y, Zr, and REE) since 12,370 ^{1}4C yr BP, Geochim. Cosmochim. Ac., 65, 2337–2360, https://doi.org/10.1016/s0016-7037(01)00586-5, 2001.

Stomp, M., Huisman, J., Stal, L. J., and Matthijs, H. C.: Colorful niches of phototrophic microorganisms shaped by vibrations of the water molecule, ISME J., 1, 271–282, https://doi.org/10.1038/ismej.2007.59, 2007.

Szidat, S., Salazar, G. A., Vogel, E., Battaglia, M., Wacker, L., Synal, H.-A., and Türler, A.: ^{14}C analysis and sample preparation at the new Bern Laboratory for the Analysis of

Radiocarbon with AMS (LARA), Radiocarbon, 56, 561–566, https://doi.org/10.1017/s0033822200049602, 2014.

Thiel, T.: Nitrogen fixation in heterocyst-forming cyanobacteria, in: Genetics and regulation of nitrogen fixation in free-living bacteria, edited by: Klipp, W., Masepohl, B., Gallon, J. R., and Newton, W. E., Springer, Dordrecht, the Netherlands, https://doi.org/10.1007/1-4020-2179-8, 73–110, 2004.

Tu, L., Gilli, A., Lotter, A. F., Vogel, H., Moyle, M., Boyle, J. F., and Grosjean, M.: The nexus among long-term changes in lake primary productivity, deep-water anoxia, and internal phosphorus loading, explored through analysis of a 15,000-year varved sediment record, Global Planet. Change, 207, 103643, https://doi.org/10.1016/j.gloplacha.2021.103643, 2021.

Újvári, G., Stevens, T., Svensson, A., Klötzli, U. S., Manning, C., Németh, T., Kovács, J., Sweeney, M. R., Gocke, M., Wiesenberg, G. L. B., Markovic, S. B., and Zech, M.: Two possible source regions for central Greenland last glacial dust, Geophys. Res. Lett., 42, 10–399, https://doi.org/10.1002/2015gl066153, 2015.

Van Raden, U. J., Colombaroli, D., Gilli, A., Schwander, J., Bernasconi, S. M., van Leeuwen, J., Leuenberger, M., and Eicher, U.: High-resolution late-glacial chronology for the Gerzensee lake record (Switzerland): δ^{18}O correlation between a Gerzensee-stack and NGRIP, Palaeogeogr. Palaeocl., 391, 13–24, https://doi.org/10.1016/j.palaeo.2012.05.017, 2013.

Vinnå, Råman, L., Medhaug, I., Schmid, M., and Bouffard, D.: The vulnerability of lakes to climate change along an altitudinal gradient, Communications Earth & Environment, 2, 35, https://doi.org/10.1038/s43247-021-00106-w, 2021.

Weber, J., Bauersachs, T., and Schwark, L.: A multiphasic Younger Dryas cold period recorded in sediments of Lake Steisslingen, SW-Germany: A biomarker perspective, Quatern. Int., 542, 121–136, https://doi.org/10.1016/j.quaint.2020.03.028, 2020.

Weltje, G. J. and Tjallingii, R.: Calibration of XRF core scanners for quantitative geochemical logging of sediment cores: Theory and application, Earth Planet. Sc. Lett., 274, 423–438. https://doi.org/10.1016/j.epsl.2008.07.054, 2008.

Westerberg, A. W.: Detection and resolution of overlapped peaks for an on-line computer system for gas chromatographs, Anal. Chem., 41, 1770–1777, https://doi.org/10.1021/ac60282a018, 1969.

Weyhenmeyer, G. A., Chukwuka, A. V., Anneville, O., Brookes, J., Carvalho, C. R., Cotner, J. B., Grossart, H.-P., Hamilton, D. P., Hanson, P. C., Hejzlar, J., Hilt, S., Hipsey, M. R., Ibelings, B. W., Jacquet, S., Kangur, K., Kragh, T., Lehner, B., Lepori, F., Lukubye, B., Marce, R., McElarney, Y., Paule-Mercado, Ma. C., North, R., Rojas-Jimenez, K., Rusak, J. A., Sharma, S., Scordo, F., de Senerpont Domis, L. N., Sø, J. S., Wood, S. (Susie) A., Xenopoulos, M. A., and Zhou, Y.: Global lake health in the Anthropocene: Societal implications and treatment strategies, Earths Future, 12, e2023ef004387, https://doi.org/10.1029/2023ef004387, 2024.

Wienhues, G., Zahajská, P., Schneider, T., Fischer, D., and Grosjean, M.: Direct detection of phycocyanin in sediments by hyperspectral imaging, J. Paleolimnol., 73, 73–87, https://doi.org/10.1007/s10933-024-00350-y, 2025.

Yabuzaki, J.: Carotenoids Database: structures, chemical finger prints and distribution among organisms, Database (Oxford), Vol. 2017, bax004, https://doi.org/10.1093/database/bax004, 2017.

Zander, P. D., Żarczyński, M., Vogel, H., Tylmann, W., Wacnik, A., Sanchini, A., and Grosjean, M.: A high-resolution record of Holocene primary productivity and water-column mixing from the varved sediments of Lake Żabińskie, Poland, Sci. Total Environ., 755, 143713, https://doi.org/10.1016/j.scitotenv.2020.143713, 2021.

Zander, P. D., Wienhues, G., and Grosjean, M.: Scanning hyperspectral imaging for in situ biogeochemical analysis of lake sediment cores: Review of recent developments, J. Imaging, 8, 58, https://doi.org/10.3390/jimaging8030058, 2022.

Zander, P. D., Wirth, S. B., Gilli, A., Peduzzi, S., and Grosjean, M.: Hyperspectral imaging sediment core scanning tracks high-resolution Holocene variations in (an)oxygenic phototrophic communities at Lake Cadagno, Swiss Alps, Biogeosciences, 20, 2221–2235, https://doi.org/10.5194/bg-20-2221-2023, 2023.

Züllig, H.: Carotenoids from plankton and photosynthetic bacteria in sediments as indicators of trophic changes in Lake Lobsigen during the last 14000 years, Hydrobiologia, 143, 315–319, https://doi.org/10.1007/978-94-009-4047-5_40, 1986.